

# Shell Model in the Complex Energy Plane

N. Michel,<sup>1,2</sup> W. Nazarewicz,<sup>3,4,5</sup> M. Płoszajczak,<sup>6</sup> T. Vertse,<sup>7,8</sup>

<sup>1</sup>Department of Physics, Graduate School of Science, Kyoto University,  
Kyoto 606-8502, Japan

<sup>2</sup>CEA/DSM/IRFU/SPhN Saclay, F-91191 Gif-sur-Yvette, France

<sup>3</sup>Department of Physics and Astronomy, University of Tennessee,  
Knoxville, TN 37996, USA

<sup>4</sup> Physics Division, Oak Ridge National Laboratory, Oak Ridge, TN 37831, USA

<sup>5</sup>Institute of Theoretical Physics, Warsaw University,  
ul. Hoża 69, PL-00681, Warsaw, Poland

<sup>6</sup> Grand Accélérateur National d'Ions Lourds (GANIL),  
CEA/DSM – CNRS/IN2P3, BP 5027, F-14076 Caen Cedex 5, France

<sup>7</sup>Institute of Nuclear Research of the Hungarian Academy of Sciences,  
H-4001 Debrecen, P. O. Box. 51, Hungary

<sup>8</sup> University of Debrecen, Faculty of Information Science,  
H-4010 Debrecen, P. O. Box. 12, Hungary

October 22, 2018

## Abstract

This work reviews foundations and applications of the complex-energy continuum shell model that provides a consistent many-body description of bound states, resonances, and scattering states. The model can be considered a quasi-stationary open quantum system extension of the standard configuration interaction approach for well-bound (closed) systems.

# Contents

<b>1</b>	<b>Introduction</b>	<b>3</b>
<b>2</b>	<b>Gamow states and the Berggren ensemble</b>	<b>4</b>
2.1	Antibound states . . . . .	5
2.2	Generalized Berggren representation . . . . .	7
2.3	Berggren completeness relation for protons . . . . .	8
2.4	Foundation of the GSM and interpretation of resonant states . . . . .	8
2.5	Applications of single-particle resonant states to various nuclear structure problems . . . . .	10
2.6	Example 1: resonant state expansions and continuum RPA . . . . .	12
2.7	Example 2: GSM for isobaric analogue resonances in Lane model . . . . .	12
<b>3</b>	<b>Complex scaling method</b>	<b>13</b>
<b>4</b>	<b>One-body space of the GSM</b>	<b>15</b>
4.1	Resonant and scattering states of generating potential . . . . .	15
4.2	Normalization of single-particle states . . . . .	16
4.3	Discretization of the scattering contour . . . . .	17
4.4	Gamow Hartree-Fock potential . . . . .	17
4.5	Numerical tests of the Berggren completeness relation . . . . .	18
<b>5</b>	<b>Gamow Shell Model</b>	<b>20</b>
5.1	Many-body GSM basis . . . . .	20
5.2	Determination of many-body resonant states . . . . .	20
5.3	GSM Hamiltonian . . . . .	21
5.4	Matrix elements of electromagnetic operators . . . . .	21
5.5	Optimization of the scattering contour of GSM using the Density Matrix Renormalization Group method . . . . .	22
<b>6</b>	<b>GSM applications</b>	<b>24</b>
6.1	GSM applications with schematic Hamiltonians . . . . .	24
6.2	GSM with realistic interactions . . . . .	25
6.3	Center-of-mass treatment in GSM . . . . .	28
6.4	Overlap integrals and spectroscopic factors in GSM . . . . .	29
6.5	Comparison between GSM and COSM for light nuclei . . . . .	31
<b>7</b>	<b>Perspectives</b>	<b>32</b>
<b>8</b>	<b>Acknowledgments</b>	<b>33</b>

# 1 Introduction

Small quantum systems, whose properties are profoundly affected by environment, i.e., continuum of scattering and decay channels, are intensely studied in various fields of physics (nuclear physics, atomic and molecular physics, nanoscience, quantum optics, etc.). These different open quantum systems (OQS), in spite of their specific features, have generic properties, which are common to all weakly bound/unbound systems close to the threshold. While many of these phenomena have been originally studied in nuclear reactions, it is not possible to experimentally control the behavior of the nucleus by varying external parameters as in, e.g., atoms and molecules, quantum dots, or microwave resonators.

Nuclear physics contains the core of sub-atomic science with the main focus on self-organization and stability of nucleonic matter. Nuclei themselves are prototypical mesoscopic OQSs and splendid laboratories of many-body physics. While the number of degrees of freedom in heavy nuclei is large, it is still very small compared to the number of electrons in a solid or atoms in a mole of gas. Nevertheless, nuclei exhibit behaviors that are emergent in nature and present in other complex systems. Since nuclear properties are profoundly affected by environment, i.e., the many-body continuum representing scattering and decay channels, a simultaneous understanding of the structural and reaction aspects is at the very heart of understanding short-lived nucleonic matter. An essential part of the motion of those exotic systems is in classically forbidden regions, and their properties are profoundly impacted by both the continuum and many-body correlations (see Fig. 1 and Ref. [1]). By studying the limits of nuclear existence, we also improve our understanding of the ordinary nuclei around us, extending the nuclear paradigm.

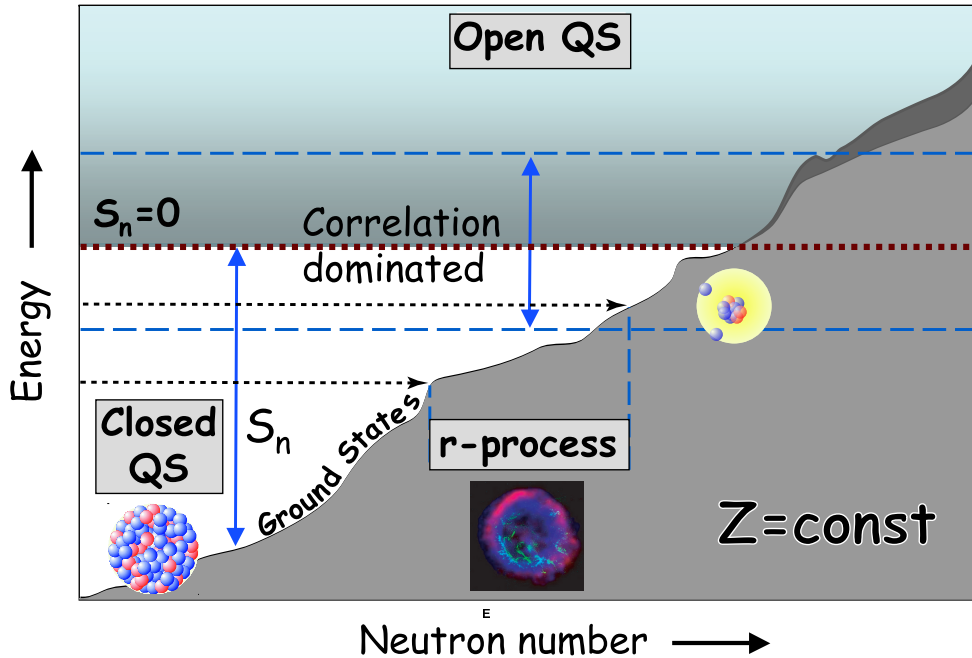


Figure 1: Schematic diagram illustrating various aspects of physics important in neutron-rich nuclei. One-neutron separation energies  $S_n$ , relative to the one-neutron drip-line limit ( $S_n=0$ ), are shown for some isotopic chain as a function of  $N$ . Weakly bound nuclei, such as halos, inhabit a drip-line region characterized by very small values of  $S_n$ . The unbound nuclei beyond the one-neutron drip line are resonances. Their widths (represented by a dark area) vary depending on their excitation energy and angular momentum. At low excitation energies, well-bound nuclei can be considered as closed quantum systems. Weakly bound and unbound nuclei are open quantum systems that are strongly coupled to the scattering environment. The regime of particularly strong many-body correlations involving weakly bound and unbound neutrons with  $|S_n| < 2$  MeV is indicated as “correlation dominated” [1]. In this region, the neutron chemical potential has the same magnitude as the neutron pairing gap. The astrophysical r-process is expected to proceed in the region of low separation energies, around 2-4 MeV. In this region, effective interactions are strongly affected by isospin, and the many-body correlations and continuum effects are essential.

Resonances are commonly found in various quantum systems, independently of their building blocks and the kinematic regime of their appearance. Resonances are genuine intrinsic properties of quantum systems, associated with their natural frequencies, and describing preferential decays of unbound states. The effect of resonances and the non-resonant scattering states can be considered in the OQS extension of the shell model (SM), the so-called continuum shell model (CSM) [2]. A particular realization of the CSM is the complex-energy CSM based on the Berggren ensemble, the Gamow Shell Model (GSM). The standard quantum mechanics (the Hilbert space formulation) does not allow the description of state vectors with exponential growth and exponential decay, such as resonance states. Since the spectrum of an observable is real in the Hilbert space, the usual procedure for treating unbound resonance states is either to extract the trace of resonances from the real-energy continuum level density or to describe the resonances by joining the *bound* state solution in the interior region with an asymptotic solution, e.g., within the R-matrix approach [3, 4].

These difficulties of the Hilbert space formulation have been resolved in the Rigged Hilbert Space (RHS) [5, 6] formulation. Thus, in a broader sense, the mathematical setting of GSM follows directly from the formulation of quantum mechanics in the RHS (Gel'fand triple) [5, 6] rather than the usual Hilbert space (see, e.g., Refs. [7, 8]). The Gel'fand triple framework allows not only to formulate rigorously Dirac's formalism of 'bras' and 'kets' [9, 10] but also encompasses new concepts, like Gamow states, and is suitable for extending the domain of quantum mechanics into the time-asymmetric processes like decays, offering a unified treatment of bound, resonance, and scattering states.

In the past, Gamow states have been discussed in various contexts [11, 12, 13, 14, 15, 16, 17, 18, 19, 20, 21, 22], including those related to the GSM works discussed in this paper. The subject of this review is to present the foundations and selected applications of the nuclear SM in the Berggren ensemble. This model provides a natural generalization of the standard nuclear SM for the description of configuration mixing in weakly bound states and resonances.

Alternative Hilbert-space-based description of the interplay between many-body scattering states, resonances, and bound states can be formulated using the concept of projected subspaces [23, 24]. Realistic studies within the real-energy CSM have been presented recently in the framework of the Shell Model Embedded in the Continuum (SMEC) [25, 26]. A phenomenological CSM with an approximate treatment of continuum couplings has been proposed in Ref. [27]. These models have the advantage of being able to provide reaction observables such as radiative capture and elastic/inelastic cross sections [25]. However, they rely on a somehow artificial separation of the Hilbert space into bound/resonant and non-resonant scattering parts. This is contrary to GSM, in which all states are treated on the same footing. The use of projected subspaces in SMEC (CSM) complicates matters significantly when several particles in the non-resonant scattering continuum are considered. It is only recently that SMEC has been extended to treat the two-particle continuum [26] in the context of two-proton radioactivity [28]. While numerically demanding, these first applications were still subject to several approximations, such as sequential or two-body cluster decays.

The paper is organized as follows. Section 2 discusses the concept of Gamow states and the Berggren basis. The complex scaling method, employed in GSM to find Gamow states and regularize integrals, is outlined in Sec. 3. Section 4 describes properties of the one-body Fock space of the GSM. The many-body GSM is described in Sec. 5, and examples of applications are given in Sec. 6. Finally, Sec. 7 outlines perspectives.

## 2 Gamow states and the Berggren ensemble

The Gamow states [29, 30] (sometimes called Siegert [11] or resonant states) were introduced for the first time in 1928 by George Gamow to describe  $\alpha$  decay. Gamow introduced complex-energy eigenstates

$$\tilde{E}_n = E_n - i \frac{\Gamma_n}{2} \quad (1)$$

in order to explain the phenomenon of particle emission in a quasi-stationary formalism [31]. Indeed, if one looks at the temporal part of a decaying state, which is  $e^{iE_0 t/\hbar} e^{-\Gamma t/(2\hbar)}$ , one notices that the squared modulus of the wave function has the time-dependence  $\propto e^{-\Gamma t}$ , and one can identify  $\Gamma$  with the decay width that defines the half-life of the state:

$$T_{1/2} = \frac{\hbar \ln 2}{\Gamma}. \quad (2)$$

The resonant states can be identified with the poles of the scattering matrix  $S(k_n)$ ,

$$\tilde{E}_n = \frac{\hbar^2}{2m} k_n^2, \quad (3)$$

in the complex-momentum plane. The bound states are thus resonant states lying on the imaginary- $k$  axis.

In 1968, Berggren proposed [32] a completeness relation for single-particle (s.p.) resonant states involving a complex-energy scattering continuum:

$$\sum_n u_n(E_n, r) u_n(E_n, r') + \int_L dE u(E, r) u(E, r') = \delta(r - r'), \quad (4)$$

where

$$u_n(E_n, r) \sim O_l(k_n r) \sim e^{i k_n r} \quad (5)$$

and  $k_n = i\kappa_n$  ( $\kappa_n > 0$ ) for bound states and  $k_n = \gamma_n - i\kappa_n$  ( $\kappa_n, \gamma_n > 0$ ) for decaying resonances in the fourth quadrant of the complex- $k$  plane.

In practical applications, it is more convenient to write (4) in momentum space:

$$\sum_{n \in (b, d)} |u_n\rangle \langle u_n| + \int_{L^+} |u(k)\rangle \langle u(k)| dk = 1. \quad (6)$$

As seen in Fig. 2, bound and quasi-bound states (e.g, resonances) enter the completeness relation (6) on the same footing. The completeness relation introduced by Berggren reduces to the traditional one involving bound and scattering states if the contour  $L^+$  lies on the real  $k$ -axis.

The radial wave functions corresponding to the  $S$ -matrix poles with  $Im(k) < 0$  diverge as  $r \rightarrow \infty$ ; hence, the scalar product among basis states has to be generalized. Firstly, a biorthogonal basis is used for the radial wave function, i.e. a different basis set for the states in bra and ket positions. Second, radial integrals have to be regularized. These extensions stem from the fact that continuum states belong to RHS. The RHS metric becomes equivalent to the ordinary metric only for bound states.

While many important developments took place prior to Berggren's work, e.g., analytic properties of the Green's function and the scattering matrix were recognized [13], and Zel'dovich [33] and Hokkyo [34] proposed regularization methods to normalize Gamow vectors; however, the bound and resonant states were thought to be non-orthogonal and this caused conceptual difficulties. In Ref. [32], Berggren applied the regularization method of Zel'dovich (with a Gaussian convergence factor) to normalize Gamow states and proved the completeness relation (4). Another type of regularization was introduced by Romo [35] who used the analytic continuation of the norm integral from the upper  $k$  halfplane to the resonant state in the lower  $k$  halfplane. As an application, he solved a two-channel problem involving a Gamow state. Zimányi introduced yet another way of normalizing Gamow states by changing the strength of the generating potential [36, 37] and applying this technique to the coupled Lane equations for complex-energy isobaric analog resonances. Bang and Zimányi used a Gamow form factor in the description of stripping reactions leading to a final resonant state [38]. In 1972, Gyarmati and Vertse [39] proved the equivalence of normalization procedures of Zel'dovich and Romo for neutron resonant states. They demonstrated the existence of the norm for a proton resonant state and introduced a new regularization procedure. This *external complex scaling* method, applied in GSM, is described in some detail in Sec. 4.2.

## 2.1 Antibound states

Antibound (or virtual) states lie on the negative semi-axis of the imaginary  $k$ :  $k_n = -i\kappa_n$  ( $\kappa_n > 0$ ) (see Fig. 2). They have real and negative energies that are located in the second Riemann sheet of the complex energy plane [40, 41, 42, 43]. Asymptotically, the radial wave function of a virtual state grows exponentially:

$$w_n(E_n, r) \sim O_l(k_n r) \sim e^{i k_n r} = e^{\kappa_n r}. \quad (7)$$

As often discussed in the literature, it is difficult to provide a physical interpretation to virtual states. In the Hilbert space formulation of quantum mechanics, a virtual state is not considered as a state but as a feature of

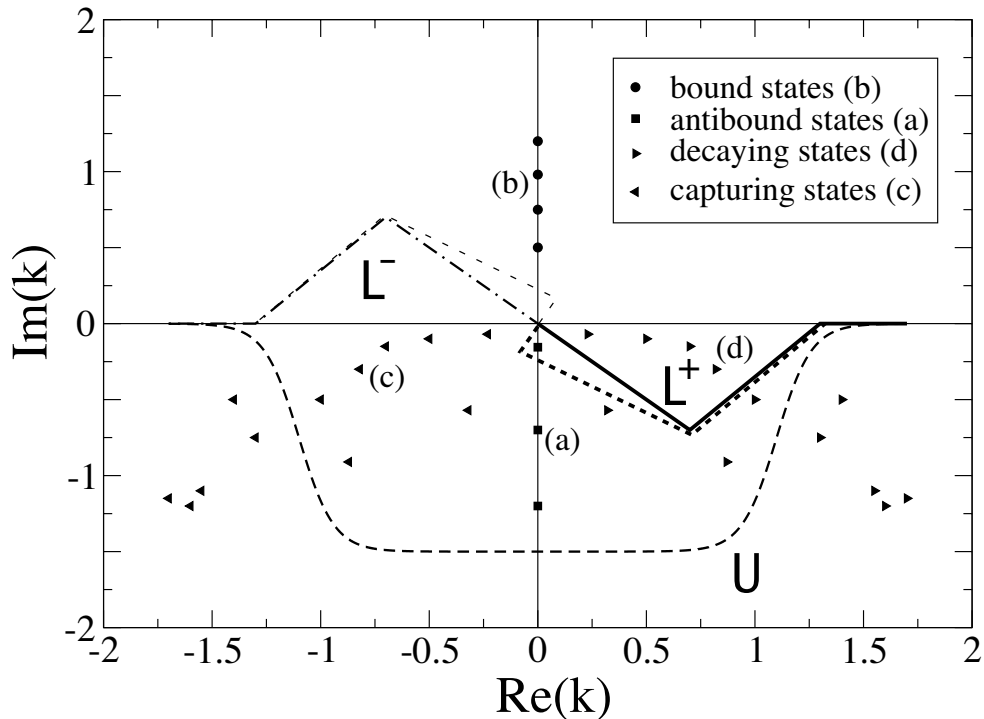


Figure 2: Location of one-body states in the complex momentum plane. The Berggren completeness relation (6) involves the bound states (b) lying on the imaginary  $k$ -axis, scattering states on the  $L^+$  contour (solid thick line), and resonant decaying states (d) in the fourth quarter of the complex- $k$  plane lying between the real axis and  $L^+$ . In the general expansion of the resolvent, the scattering states along the  $U$  contour and all resonant states lying above  $U$  are included. The antibound states (a) can be included in the generalized completeness relation; in this case the contour  $L^+$  has to be slightly deformed (dashed thick line).

the system (as the second energy sheet is considered unphysical and inaccessible through direct experiments). In the RHS formulation, the virtual state can be interpreted both as a vector in the RHS and as a pole of the  $S$ -matrix. The latter implies that virtual states can be “seen” only close to the threshold; they manifest themselves in an increased localization of low-energy scattering states. Consequently, the presence of a virtual state at a sufficiently small energy has an appreciable influence on the scattering length and the low energy scattering cross section. Classic examples include the low-energy  $\ell=0$  nucleon-nucleon scattering characterized by a large and negative scattering length [42, 44]. Related to this is an increased localization of real-energy scattering states just above threshold [45].

It is instructive to study the energies of antibound states as a function of potential parameters. A detailed study of this problem was done by Nussenzveig [46] (see also Ref. [47] for a discussion of the one-dimensional case). To this end, it is convenient to fix the geometry (radius and diffuseness) of the potential and follow the trajectories of the bound and antibound poles as a function of the well depth  $V_0 > 0$ . If there is no potential barrier, e.g., for  $s$ -wave neutrons, no narrow resonances appear. Here, by increasing  $V_0$  from the minimal value at which the antibound state appears, the pole goes across  $k = 0$ , forming a bound state with a radial wave function having one node,  $n = 1$ . For protons or for  $l > 0$  neutrons, a potential barrier is present which can support resonant poles. In this case, decaying and capturing poles appear in pairs which move towards the imaginary  $k$ -axis as  $V_0$  increases. At certain values of  $V_0$  the poles meet at  $k=0$ , forming a double singularity. For still larger values of  $V_0$ , one of the poles becomes a bound state, while the other one moves down as an antibound state.

Neutron  $l=0$  pole trajectories are shown in Fig. 3 as a function of  $V_0$  for a square well potential. The behavior of the antibound poles conforms to the general pattern discussed above. Namely, below  $V_0 = 1.05$  MeV, there appears only one antibound state. This pole moves to the upper half  $k$ -plane and forms a bound state with one node. By increasing the depth further from  $V_0 = 9.05$  MeV, there appear two antibound poles.

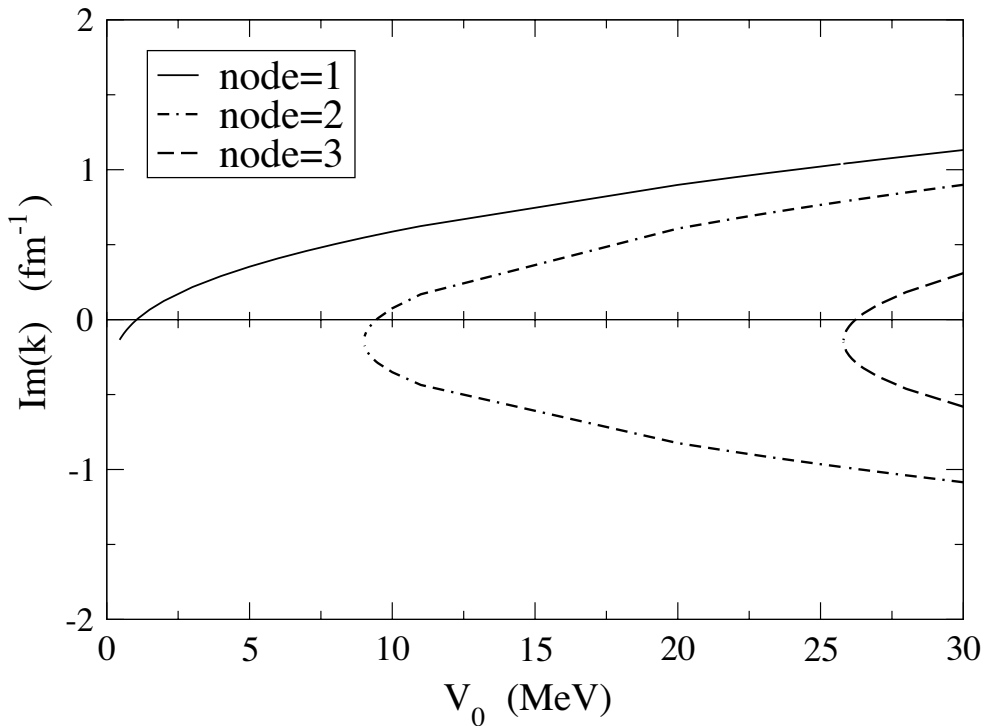


Figure 3: Positions of the bound and antibound neutron  $l=0$  poles with  $n=1,2,3$  radial nodes on the imaginary  $k$ -axis as a function of the depth  $V_0$  of the square well potential with radius  $R = 7$  fm.

One of them moves upwards and at about  $V_0 = 9.5$  MeV, it emerges as a  $2s$  bound state, while the other one moves down and remains antibound. At about  $V_0 = 26$  MeV three antibound and two bound states are present. By increasing  $V_0$  to 30 MeV, the antibound pole lying closest to the origin becomes bound, resulting in three bound and two antibound states. At  $V_0=30$  MeV, the  $3s$  bound state is closer to the origin than the corresponding antibound pole. Therefore, there are no antibound poles between the loosest bound state and the threshold [40]. For the cases with a non-zero barrier, the resonant poles meet in the origin and one obtains a similar pattern as in Fig. (3) but with the  $\text{Im}(k)$ -axis shifted down by about  $k = 0.15$  fm $^{-1}$ . This shift would change the relative distance of the antibound and bound states with respect to the origin, with one antibound pole to appear between the loosest bound state and the threshold [40].

## 2.2 Generalized Berggren representation

In the original formulation of the completeness relation (6), only decaying poles with

$$\arg(k_n) > -\frac{\pi}{4}, \quad \text{Re}(E_n) > 0 \quad (8)$$

were considered. Consequently, virtual resonances (resonant poles with  $\text{Re}(E_n) < 0$ ) and antibound states were excluded from the Berggren ensemble. The Berggren representation has been generalized in Ref. [48] by including a virtual state into the discrete part of the basis. The generalization requires a slight deformation of  $L^+$  as indicated in Fig. 2. More recently, this generalized Berggren representation was used in a full form (i.e., including the scattering component) for the description of drip-line nuclei  $^{11}\text{Li}$  and  $^{72}\text{Ca}$  [49, 50]. A large destructive interference between the virtual state and the scattering contour states has been observed. In this picture, the bound ground state of  $^{11}\text{Li}$  could be explained in terms of unbound states of  $^{10}\text{Li}$ . Soon afterwards it was noted [51] that a generalized Berggren basis is not optimal as far as the number of basis states is concerned. Indeed, as the halo wave function has a decaying character at large distances due to the exponentially increasing asymptotics of the virtual state (7), its inclusion in the basis always induces strong negative interference with the scattering states. Therefore, adding antibound states to the basis is not beneficial in GSM applications, as more discretized scattering states are necessary to reach a required precision.

### 2.3 Berggren completeness relation for protons

The completeness relation by Berggren (6) can be derived from the Newton completeness relation for the set of real-energy eigenstates of a short-range potential [40]:

$$\sum_{n \in (b)} |u_n\rangle\langle u_n| + \int_0^{+\infty} |u(k)\rangle\langle u(k)| dk = 1. \quad (9)$$

The proof can be carried out by deforming the real momentum axis associated with positive-energy scattering states into the  $L^+$  contour of Fig. 2 and applying the Cauchy integral theorem [14]. This is possible because resonant states appear as residues, due to their  $S$ -matrix pole character.

Bound and real-energy scattering states generated by a potential bearing a Coulomb tail naturally form a complete set as well, as all self-adjoint operators possess a spectral decomposition [52]. However, methods used in Ref. [52], relying on the Lebesgue measure theory, are very general and fairly abstract. Thus, a simple demonstration of the completeness relation for potentials with a pure Coulomb asymptotic behavior is called for. The proof of (9) relies on the analyticity of the Green's function of a local potential that is integrable for  $r \rightarrow +\infty$  [40]. Potentials having a Coulomb tail, proportional to  $r^{-1}$ , have not been considered in Ref. [40]. Moreover, non-locality often appears in practical applications [53], so it is important to demonstrate the completeness relation for non-local potentials having a Coulomb asymptotic behavior. This has been done recently in Refs. [53, 54], where detailed derivations can be found.

In short, the main assumption behind the proof presented in Refs. [53, 54] is that beyond a finite radius  $R_0$  the potential behaves as  $r^{-1}$ . The corresponding radial Schrödinger equation reads:

$$u''(k, r) = \left( \frac{\ell(\ell+1)}{r^2} + v(r) - k^2 \right) u(k, r) + \int_0^{R_0} w(r, r') u(k, r') dr', \quad (10)$$

where  $v(r)$  and  $w(r, r')$  are respectively the local and non-local potentials. For  $r > R_0$ , the wave function is a linear combination of regular and irregular Coulomb functions. Their analytical character and the fact that regular Coulomb wave functions form a complete set [54, 55, 56] are important to the demonstration of the completeness. Using analytic continuation arguments, one can also demonstrate that the set of bound and real-energy scattering states generated by complex potentials  $v(r)$  and  $w(r, r')$  is complete, provided no exceptional points, i.e., bound states of norm zero [57], are present.

### 2.4 Foundation of the GSM and interpretation of resonant states

Heuristic methods often precede a complete formulation of the physical theory in terms of an adequate mathematical apparatus. This was the case for Dirac's formulation of quantum mechanics [58] which a posteriori found a satisfactory setting in the RHS [9, 10]. This is also the case for theoretical developments utilizing Gamow states to describe weakly bound and/or unbound states of quantum systems. The Berggren completeness relation [32], which replaces the real-energy scattering states by the resonance contribution and a background of complex-energy continuum states, puts the resonance part of the spectrum on the same footing as the bound and scattering spectrum. However, resonances do not belong to the usual Hilbert space, so the mathematical apparatus of quantum mechanics in Hilbert space is inappropriate and cannot encompass concepts such as Gamow states. Quite unexpectedly, it turned out that the mathematical structure of the RHS is ready to extend the domain of quantum mechanics into the time-asymmetric processes such as decays.

The RHS, or Gel'fand triple, is a triad of spaces [5, 6, 59]:

$$\Phi \subset \mathcal{H} \subset \Phi^\times, \quad (11)$$

which represent different completions of the same infinitely dimensional linear space  $\Psi$ .  $\Phi$  (the subspace of test functions) is a dense subspace of Hilbert space  $\mathcal{H}$ , and  $\Phi^\times$  (the space of distributions) is the space of antilinear functionals over  $\Phi$ .  $\Phi$  is also the largest subspace of  $\mathcal{H}$  on which expectation values, uncertainties and commutation relations can be correctly defined for unbounded operators.

The linear functionals over  $\Phi$  are contained in the space  $\Phi'$  which is related to another RHS:

$$\Phi \subset \mathcal{H} \subset \Phi' . \quad (12)$$



One should stress that  $\mathcal{H}$  in (11) and (12) does not have any particular significance in the RHS formalism. For all physics problems, one needs only the dual pair of spaces  $\Phi \subset \Phi^\times$  which characterize the considered quantum system. For example, bras and kets, which are related to the continuous part of the spectrum of an observable, belong to  $\Phi'$  and  $\Phi^\times$ , respectively, and not to  $\mathcal{H}$ . Apparently, the RHS provides also a more convenient framework than  $\mathcal{H}$  to capture physical principles of quantum mechanics. The Heisenberg's uncertainty relations are properly defined on  $\Phi$ , and not on  $\mathcal{H}$ .

Besides implementation of Dirac's formalism of bras and kets, the RHS provides a framework for a quantum mechanical description of common irreversible processes, like the formation or decay of quantum states. Indeed,  $\Phi^\times$  may contain generalized eigenvectors of the observable(s) with complex eigenvalues. The generalized eigenvectors of the Hermitian Hamiltonian are Gamow vectors. Examples of the RHS for the observables having a continuous part in the spectrum can be found, for example, in Refs. [60, 22].

Gamow vectors are state vectors of resonances. They belong to RHS and not to  $\mathcal{H}$  since the self-adjoint operators in  $\mathcal{H}$  can only have real eigenvalues. Like the plane waves (the Dirac kets), the Gamow functions are not square integrable and must be treated as distributions. In this way, one succeeds to generate Gamow bras and kets which fit naturally in the RHS. However, unlike the Dirac kets, the probability density for Gamow functions is not constant but increases exponentially in space.

Rules for the normalization of Gamow functions and corresponding completeness relations have been proposed [34, 32, 35, 61, 62, 39] independently of the RHS formulation. Similarly, the momentum space representation for Gamow functions has been introduced [63, 64]. RHS offers a mathematical framework to formulate those results rigorously. In particular, the RHS provides a unifying dual description of bound, resonant and scattering states both in terms of the  $S$ -matrix and in terms of the vector in the RHS. The transition amplitude  $\mathcal{A}(E_n \rightarrow E)$  from a resonance of energy  $E_n$  to a scattering state at an energy  $E$  ( $E \geq 0$ ) [22]:

$$\mathcal{A}(E_n \rightarrow E) = i\sqrt{2\pi}N_n\delta(E - E_n), \quad (13)$$

where  $N_n$  denotes the normalization factor, is proportional to the complex  $\delta$ -function [65] which, far off the threshold energy in the region of the resonance, can be approximated by the Breit-Wigner amplitude. This physically expected result provides a formal link between Gamow states and nearly-Lorentzian peaks in cross-sections for narrow, isolated resonances.

Interpretation of certain aspects of the RHS formulation of quantum mechanics is still debated, and connections between Berggren and RHS formulations continue to be studied (for a recent review, see [60]). One aspect of this discussion concerns complex matrix elements of the operators and probabilistic interpretation of the resonant wave function. As an illustration of this problem for resonances, let us consider the solution of the Schrödinger equation  $\chi(\mathbf{r}, t)$  for a s.p. Hamiltonian  $\hat{h}$ :

$$i\hbar\frac{\partial}{\partial t}\chi(\mathbf{r}, t) = \hat{h}\chi(\mathbf{r}, t). \quad (14)$$

In the stationary picture, the resonant wave function is the product of time-dependent  $\tau(t)$  and space-dependent  $\psi(\mathbf{r})$  factors:

$$\chi(\mathbf{r}, t) = \tau(t)\psi(\mathbf{r}), \quad (15)$$

where the time-dependent factor is:

$$\tau(t) = e^{-i\frac{\tilde{E}_n}{\hbar}t}. \quad (16)$$

The complex energy  $\tilde{E}_n$  (1) is the generalized eigenvalue of  $\hat{h}$  with the complex wave number  $k_n$  (3). The corresponding space-dependent eigenfunction  $\psi(\mathbf{r}, k_n)$ ,

$$\psi_n = \psi_{n\ell jm}(\mathbf{r}, k_n) = \frac{u_{n\ell j}(k_n, r)}{r} [Y_\ell(\hat{r})\chi_s]_{jm}, \quad (17)$$

satisfies an outgoing wave boundary condition. At large distances, the radial part of the  $\ell=0$  wave function is proportional to  $\exp(ik_n r)$ . For a decaying resonance,  $k_n = \gamma_n - i\kappa_n$  ( $\gamma_n, \kappa_n > 0$ ), the time-dependent factor

$$\tau(t) = e^{-i\frac{\tilde{E}_n}{\hbar}t} = e^{-i\frac{E_n}{\hbar}t} e^{-\frac{\Gamma_n}{2\hbar}t}, \quad (18)$$

describes an exponential decay with a decay width  $\Gamma_n$ . As  $r$  increases, the radial part of  $\psi(\mathbf{r}, k_n)$  oscillates with an exponentially growing amplitude:

$$e^{ik_n r} = e^{i\gamma_n r} e^{\kappa_n r} = [\cos(\gamma_n r) + i \sin(\gamma_n r)] e^{\kappa_n r} . \quad (19)$$

The decay process in this picture is unlimited in both time ( $t \in [0, \infty]$ ) and space ( $r \in [0, \infty]$ ) and, henceforth, continues forever. This feature guarantees, in fact, the particle-number conservation [66]: the exponential temporal decrease of the wave function amplitude is complemented by its exponential spatial increase, and the divergence of the resonance wave function assures that the particle number is conserved.

In general, the quasi-stationary description of a time-dependent physical process works well when the decaying state is narrow, as in this case the formation of a state and its subsequent decay can be well separated in time. A narrow Gamow resonance has a large overlap with a properly shaped wave packet [67] and its radial wave function is similar to a bound state wave function while the imaginary part is small inside the nucleus. In the reaction cross section, such a narrow resonance shows up as a sharp peak which can be well separated from the non-resonant background.

Another aspect of the debate on the physical interpretation of Gamow vectors concerns the expectation value of an operator in a resonant state. Berggren's interpretation of real and imaginary parts of the expectation value of an operator is based on the discussion of interference effects in the reaction cross-sections [68]. Berggren showed that the imaginary part of the complex cross section calculated with the Gamow resonance as a final state describes the interference of that resonance with the non-resonant background. In a later paper [69], Berggren demonstrated that for any operator which commutes with the Hamiltonian, the expectation value of that operator is the real part of its matrix element, and the negative of the square of the imaginary part of the matrix element can be associated with the square of an uncertainty of the expectation value. This proof holds only for operators which commute with the Hamiltonian. It turns out that the Berggren interpretation of the expectation value [69] is largely equivalent to the RHS formulation by Bohm and Gadella [70] and coincides with it in the leading order [15, 71].

The meaning of a complex radial expectation value was studied in Ref. [72] using a model of two coupled channels [73]. It was found that the radial expectation value in this model can be interpreted according to Berggren's prescription and that it can be used to characterize the resonances as long as the wavelength of the decaying wave is shorter than the radial extension of the resonant state.

## 2.5 Applications of single-particle resonant states to various nuclear structure problems

Already in 1970, in the pioneering work employing resonant states, a truncated resonant basis composed of bound neutron and resonant proton states was used to describe isobaric analog resonances [37]. The pole expansion of the radial wave function, the Green's function, and the scattering matrix were subsequently discussed in a rigorous way in Ref. [74] by using the Mittag-Leffler (ML) expansion. They used the normalization of the pole solutions introduced in [34] and later employed in, e.g., Refs. [61, 75]. The authors of Ref. [74] suggested that the pole expansion could be used in (shell-model-type) nuclear structure calculations; however, they worried about the non-orthogonality of the basis. In a numerical study [76], the usefulness of the ML-type pole expansion of the Green's function was examined. The question of overcompleteness was finally put to rest by Berggren and Lind [77].

Resonant state expansions were also used by atomic physicists for calculating the  $S$ -matrix, expressed as a sum of pole terms and a contour integral [78]. The positions of the poles were calculated by using the uniform complex scaling (see Sec. 3), while the residues were obtained by using numerical methods described in Refs. [79, 80]. Neutron emission from a heavy-ion reaction was modeled in a time-dependent two-center shell model in Ref. [81]. Therein, resonant states were calculated in the momentum space using the potential separable expansion (PSE) method [82, 83], in which the potential is expanded in a square integrable (harmonic oscillator; HO) basis, and the proper asymptotic of the wave function is guaranteed by the presence of the free Green's function.

A less severe truncation of the Berggren basis was employed in the late 1980s in the resonant approach to the random phase approximation (RRPA), in which the contribution from the non-resonant continuum was neglected [84, 85]. Such an expansion is usually referred to as a *pole approximation*. (A detailed summary

of the early theoretical approaches employing resonant states can be found in Ref. [86].) A similar pole approximation was used in the RRPA description of giant resonance escape widths [87]. A careful test of different pole expansions was carried out in Ref. [76] by using a benchmark continuum RPA result for the particle-hole response function (see Sec. 2.6 for details). It was found that the ML-type pole expansion was closer to the continuum RPA, based on the Green's function, than the pole approximation. This result was explained by Berggren and Lind [77] who identified the ML-type pole expansion of the resolvent by using the so-called  $U$  contour (see Fig. 2) in the complex  $k$ -plane. Unfortunately, an expansion using the  $U$  contour,

$$1 = \frac{1}{2} \sum_{i=a,b,c,d} |u_i\rangle\langle\tilde{u}_i| + \frac{1}{\pi} \int_U |u(k)\rangle dk \langle u(k^*)|, \quad (20)$$

cannot be used in shell-model-like calculations because the factor  $1/2$  in the front of the sum over the resonant (bound, antibound, capturing, and decaying) states destroys the idempotency of the unity operator [88]. In addition, pole expansions of type (20) are accurate only if very many poles (up to some large energy cut-off) are included in the sum; contributions from broad and virtual resonances (having negative real energies) are in fact essential [88].

In Ref. [89], Gamow states were expanded in a finite  $r \in [0, R_o]$  interval by using a finite number of square integrable basis states, called *Siegert pseudostates* (SPS). The expansion coefficients were determined by solving a normal eigenvalue problem where the dimension of the system has been doubled. This doubled system represents an eigenvalue problem with a weight matrix of the Bloch operator. The weight matrix allows the continuation of the SPS into the tail region and defines a special inner product in which a completeness relation can be constructed for the SPS. A pole expansion of the Green's function, similar to the ML expansion of Ref. [88], was carried out. This expansion was further exploited in Ref. [90]. The usefulness of SPS was further demonstrated in studies of time evolution of an infinitely extended system [91].

The resonant and continuum components of the strength function were calculated by using the Berggren completeness relation in studies of Coulomb breakup of  $^{11}\text{Be}$  [92]. They found the non-resonant contribution of the part of the contour which returns to the real  $k$ -axis negligible. A similar result was obtained in Ref. [93].

In some of the pole expansions mentioned above, complex eigenvalues and radial wave functions of resonant states were calculated using the code GAMOW [94]. Later, more efficient numerical techniques have been used based on the piecewise perturbation method [95, 96]. In other work [97] spherical resonant states were obtained by solving a non-linear set of equations. Bound and resonant state energies were calculated in code PSEUDO by using the PSE method in [98] for an axially symmetric potential by finding the zeroes of the Fredholm determinant of the Lippmann-Schwinger equation. Recently a method was developed in which the momentum-space Schrödinger equation was solved by a contour deformation method [93].

More recent applications of pole expansions include a description of giant multipole resonances [99] (see Sec. 2.6), and partial decay widths corresponding to the proton decay from the Gamow-Teller and isobaric analog state resonances [100]. The Berggren representation in its full form, including the complex scattering continuum, was employed in Ref. [101] to describe the eigenstates of a realistic one-body nuclear Hamiltonian. In this work, eigenstates of a spherical symmetric potential were expanded in a full Berggren basis of a different potential. (Examples of such expansions are presented in Sec. 4.5.) The full Berggren ensemble was employed in studies of the average s.p. level density [102] and shell corrections [103, 104]. Quasiparticle resonances can be constructed from the Gamow resonances in the BCS approximation by generalizing the standard BCS to the complex energy plane if the contour integral is neglected. If the non-resonant contribution is included, the contribution from the continuum level density has to be added [105] when calculating the particle number. However, a proper description of pairing correlations in weakly bound systems must go beyond the BCS approximation [106]. Here, the tool of choice is the Gamow-HFB method to be mentioned in Sec 4.4.

Gamow states and resonant expansions have been extensively used in the description of alpha, proton, and neutron emission from nuclei. For very narrow alpha and proton resonances, a single-channel Gamow approximation that ignores the non-resonant background is fully adequate [107, 108]. An attempt was made to calculate resonant states of a deformed potential by means of an expansion in a spherical Berggren basis [109, 110]. However, for a description of narrow proton resonances in deformed nuclei, the accuracy of spherical expansion turned out to be not satisfactory and alternative approaches were used. One of them was the direct numerical integration of the set of coupled differential equations using the piecewise perturbation method.

The resulting code CCGAMOW was employed in Ref. [111] to explain full and partial decay widths of protons from axially symmetric nuclei within an adiabatic approach that ignores the rotational excitations of the daughter system. A full non-adiabatic description of proton emitters was carried out in Refs. [112, 113] using a modified version of the coupled channels program NONADI, and the extension to the triaxial case can be found in Ref. [114]. A shell-model analysis of the proton emission from  $^{31}\text{Cl}$  using Gamow wave functions was performed in Ref. [115]. In a study of Ref. [116], Gamow states were used to benchmark a modified two-potential approach to tunneling problems.

The applications of resonant states mentioned so far were concerned with the s.p. space. By 2003, however, it became possible to apply the Berggren ensemble to a general many-body case. In two parallel studies [117, 118], based on a configuration mixing approach employing the one-body Berggren ensemble, two-particle resonances in  $^{80}\text{Ni}$  and  $^{102}\text{Te}$  were calculated using separable multipole interactions [117], and systematic calculations for the neutron-rich nuclei  $^{6-10}\text{He}$  and  $^{18-22}\text{O}$  were carried out using the surface-delta interaction [119]. More applications soon followed (see Sec. 6). In the following, we shall refer to these two realizations of the SM in the complex energy plane as the Gamow Shell Model since the underlying concept is the same.

## 2.6 Example 1: resonant state expansions and continuum RPA

Continuum RPA (CRPA) is a useful tool for testing the usefulness and accuracy of resonant state expansions. For separable multipole-multipole interactions, the solution of the CRPA equations is obtained by finding complex roots of the corresponding dispersion relation [76, 99]. Complex energy poles of the particle-hole response  $R(E)$  yield positions and full widths of the correlated resonances while the partial decay widths of these states can be obtained from the associated residua.

Within CRPA, the particle Green's function in a selected partial wave is

$$g(r, r', k) = -\frac{u(k, r_{<}) v(k, r_{>})}{W(u, v)}, \quad (21)$$

where  $W$  denotes the Wronskian of the regular  $u(k, r)$  and irregular  $v(k, r)$  solutions at  $r_{<} = \min(r, r')$  and  $r_{>} = \max(r, r')$ , respectively, at real values of  $k$ . In the standard Berggren expansion using the  $L$  contour of Fig. 2, the corresponding Green's function can be written as:

$$g_L(r, r', k) = \sum_{i=b,d} \frac{u_i(k_i, r) u_i(k_i, r')}{k^2 - k_i^2} + \frac{1}{\pi} \int_L \frac{u(q, r) u(q, r')}{q(k - q)} dq. \quad (22)$$

On the other hand, if one uses the  $U$  contour of Fig. 2, the Green's function takes the form:

$$g_U(r, r', k) = \sum_{i=a,b,d,c} \frac{u_i(k_i, r) u_i(k_i, r')}{2k_i(k - k_i)} + \frac{1}{\pi} \int_U \frac{u(q, r) u(q, r')}{q(k - q)} dq. \quad (23)$$

The two complex-energy representations of Green's function given by Eqs. (22,23) and the real-energy expression (21) are mathematically equivalent; hence, they should give the same results in practical applications.

From a practical point of view, it is interesting to know if one can choose the complex contours in such a way that the contributions from the integrals in Eqs. (22) and (23) become negligible. This has been checked in Ref. [76], in which the particle-hole response functions were calculated for a square-well potential supplemented by the Coulomb field. For narrow and isolated resonances, the partial widths obtained by using the leading pole term in Eqs. (22) and (23) agree with the exact result within 10%. The subsequent calculations of Refs. [88, 99] using the Woods-Saxon potential demonstrated that the contribution from the  $U$  contour to the p-h response function could be further reduced but this does not hold for the  $L$  contour. Furthermore, it was shown [77, 14] that neglecting the integral in Eq. (22) destroys the symmetry of the resolvent and causes an artificial threshold behavior of the Green's function.

## 2.7 Example 2: GSM for isobaric analogue resonances in Lane model

The isobaric analogue resonance (IAR) can be described phenomenologically by the coupled-channel Lane equations (CCLE) [4]. The IAR-CCLE problem offers an excellent opportunity to compare the complex-energy

GSM approach with the standard CCLE solution along the real energy axis. Such a test has been carried out in Ref. [120] for the Lane Hamiltonian. Within CCLE, the multichannel Schrödinger equation has been solved by a direct numerical integration. The resulting proton scattering  $S$ -matrix has been calculated along the real energy axis in the region of the IAR and then fitted by using a single pole approximation,

$$S(E_p) = e^{2i\delta_p(E_p)} \left( 1 - i \frac{\Gamma}{E_p - \mathcal{E}_{IAR}} \right), \quad (24)$$

to determine the position  $E_r$  and width  $\Gamma$  of the IAR. In Eq. (24), the background phase shift  $\delta_p(E_p)$  was assumed to have a linear energy dependence in order to better reproduce the non-resonant background. The best fit parameter values, denoted by  $E_r(CCLE)$  and  $\Gamma(CCLE)$ , are listed in Table 1. They coincide with the GSM eigenvalue  $\mathcal{E}_{IAR} = E_r(GSM) - i \frac{\Gamma(GSM)}{2}$  within 1 keV even for the broad states. The integrated effect of

$l j$	$E_r(GSM)$	$E_r(CCLE)$	$\Gamma(GSM)$	$\Gamma(CCLE)$
$d_{5/2}$	16.445	16.444	0.141	0.140
$s_{1/2}$	16.918	16.917	0.156	0.156
$d_{3/2}$	17.441	17.440	0.144	0.145

Table 1: Comparison of the IAR parameters calculated by using CCLE and GSM for three partial waves. All energies are in MeV.

the proton continuum along the complex path is small but essential to yield the correct value of  $\Gamma(GSM)$ .

### 3 Complex scaling method

Another approach that employs the concept of complex energies and distorted contour is the complex scaling method (CS). Some aspects of the CS formalism, e.g., the use of complex coordinates, are very relevant to the GSM. For a comprehensive review of the CS method, we refer the reader to Reinhardt [121]. Below only the most essential facts are summarized.

Within CS, like in GSM, the resonances are represented by poles of the scattering matrix  $S(k)$ . By making use of the CS transformation on particle coordinates,

$$\mathbf{r} \rightarrow e^{i\theta} \mathbf{r}, \quad (25)$$

one guarantees that wave functions of the selected resonances become square integrable [122, 123, 124]. A unitary CS operator  $\hat{U}(\theta)$  acting on a s.p. wave function gives:

$$\hat{U}(\theta)\psi(\mathbf{r}) = e^{i\frac{3}{2}\theta}\psi(\mathbf{r}e^{i\theta}), \quad (26)$$

where the factor  $e^{i\frac{3}{2}\theta}$  comes from the three-dimensional volume element [121]. Under  $\hat{U}(\theta)$ , the Hamiltonian transforms as

$$\hat{h}_\theta(\mathbf{r}) = \hat{U}(\theta)\hat{h}(\mathbf{r})\hat{U}(\theta)^{-1}. \quad (27)$$

(This variant of CS is referred to as *uniform complex scaling*; it is to be distinguished from the *exterior complex scaling* discussed below.) The transformed Hamiltonian  $\hat{h}_\theta$  is no longer hermitian as it acquires a complex potential. However, for a wide class of local and nonlocal potentials, called *dilation-analytic potentials*, the so-called ABC theorem [122, 123, 124]) is valid. This theorem states that:

- i. The bound states of  $\hat{h}$  and  $\hat{h}_\theta$  are the same;
- ii. The positive-energy spectrum of the original Hamiltonian  $\hat{h}$  is rotated down by an angle of  $2\theta$  into the complex-energy plane, exposing a higher Riemann sheet of the resolvent;
- iii. The resonant states of  $\hat{h}$  with eigenvalues  $\tilde{E}_n$  satisfying the condition  $|\arg(\tilde{E}_n)| < 2\theta$  are also eigenvalues of  $\hat{h}_\theta$  and their wave functions are square integrable (see Fig. 4).

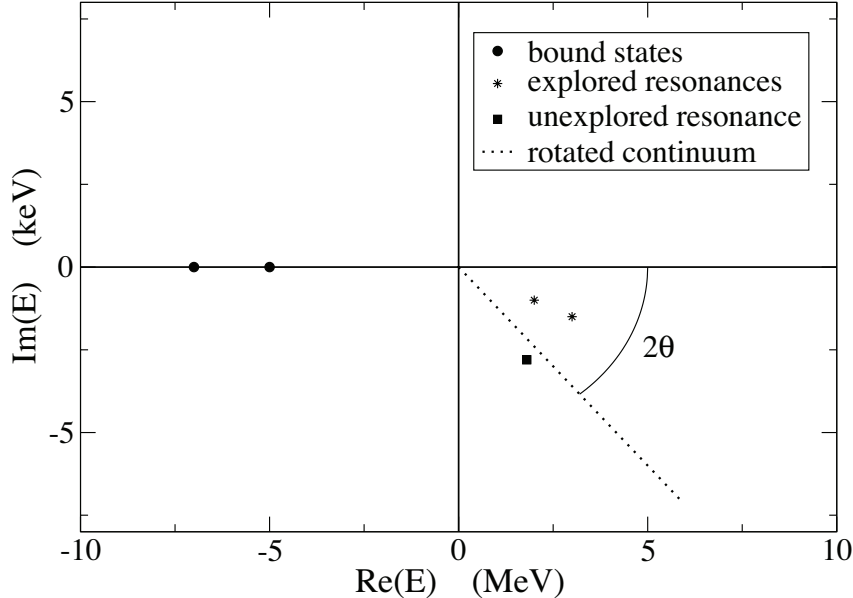


Figure 4: The complex energy plane showing bound poles (dots), resonant poles exposed by the complex scaling transformation (asterisks), the rotated continuum of the scattering states (dotted line), and a hidden pole (marked by a square; not exposed by the CS transformation). According to the ABC theorem, the eigenfunction of the exposed poles are square integrable.

Unfortunately, some of the phenomenological potentials widely used in nuclear physics are not dilatation-analytic (e.g., the Coulomb potential of a uniformly charged sphere) or they are dilatation-analytic only in a limited range of  $\theta$ . For instance, the commonly used Woods-Saxon potential and its derivative are dilatation-analytic only for  $\theta < \theta_c = \text{arctg}(\frac{a\pi}{R})$ . Some of these difficulties, however, can be cured by the use of the *exterior complex scaling* (ECS), originally introduced in Ref. [39] to prove the existence of the norm of a Gamow resonance for charged particles (see also Ref. [125]). Within ECS, the rotation of  $r$  to the complex starts at a finite distance  $r_a$  at or beyond the range of the nuclear potentials  $r_a \geq R$ . The operator  $\hat{U}_a(\theta)$  of the exterior complex scaling is defined for a wave function  $\psi(r)$  by

$$\hat{U}_a(\theta)\psi(r) = \begin{cases} \psi(r) & , \text{ if } r \leq r_a \\ \psi(r_a + |r - r_a|e^{i\theta}) & , \text{ if } |r| > r_a \end{cases} \quad (28)$$

The ECS influences only the asymptotic behavior of functions and can be applied to any finite range potential, including the Coulomb potential in the region where it behaves as  $r^{-1}$ .

The Berggren ensemble used in GSM contains non square-integrable functions; hence, a regularization procedure is needed to calculate norms and matrix elements needed in the GSM. The ECS can be used for this purpose. The complex-scaled states have square integrable wave functions and all related integrals are finite. Since the resulting matrix elements are independent of the angle, they can be calculated at any convenient value of  $\theta$ . However, if one is interested in the radial dependence of the wave function for real  $r$  (e.g., to estimate partial widths), the CS transformation needs to be inverted,

$$\psi = \hat{U}(\theta)^{-1}\psi_\theta. \quad (29)$$

Such a back rotation can introduce large errors [126] if the solution is expanded and approximated by a finite number of terms. If Padé approximants are used for performing back rotation [127], good accuracy can be achieved for narrow resonances. A comparison of the diagonalization in a Berggren basis and the CS method resulted in excellent agreement for the complex energy of the IAR in the Lane model [120].

The CS and ECS methods have been widely used in many-body calculations of unbound states and in the description of atomic and nuclear reactions, see, e.g., Refs. [128, 129, 130, 131, 132, 133, 134, 135, 136]. For recent nuclear examples, see also Sec. 7.

## 4 One-body space of the GSM

This Section describes the s.p. space of the GSM, i.e., the resonant and complex- $k$  scattering states generated by an auxiliary s.p. Hamiltonian. We describe the normalization procedure for the continuum states and discuss the discretization of the scattering contour. The optimal basis-generating potential is obtained from the Hartree-Fock procedure generalized to resonant states. Finally, selected examples of expansions in the Berggren basis are given. They nicely demonstrate the completeness of the Berggren ensemble and the accuracy of calculations.

### 4.1 Resonant and scattering states of generating potential

The radial s.p. wave functions  $u(k, r)$  that enter the Berggren ensemble (6) are solutions of the radial Schrödinger equation:

$$\frac{d^2 u(k, r)}{dr^2} = \left( \frac{\ell(\ell + 1)}{r^2} + \frac{2m}{\hbar^2} V(r) - k^2 \right) u(k, r), \quad (30)$$

where  $\ell$  is the orbital angular momentum,  $m$  is the reduced mass of the nucleon, and  $V(r)$  is the one-body potential that generates the basis. The choice of the potential is in principle arbitrary, but in practice, one is trying to optimize it by adjusting its parameters to experimental s.p. states. Another option to calculate it is using the Hartree-Fock (HF) method, as discussed in Sec. 4.4.

In many applications, a Woods-Saxon (WS) central field is used, supplemented by the spin-orbit and Coulomb potentials:

$$V(r) = -V_0 f(r) - 4V_{so}(\mathbf{l} \cdot \mathbf{s}) \frac{1}{r} \left| \frac{df(r)}{dr} \right| + V_c(r), \quad (31)$$

where

$$f(r) = \begin{cases} \left[ 1 + \exp\left(\frac{r-R_0}{d}\right) \right]^{-1} & , \text{ if } r < R \\ 0 & , \text{ if } r \geq R \end{cases}, \quad (32)$$

is a WS form-factor,  $V_0$  is the WS potential strength,  $R_0$  is the radius,  $d$  is the WS potential diffuseness,  $R$  is a cutoff radius,  $V_{so}$  is the spin-orbit coupling strength, and  $V_c(r)$  is the Coulomb potential for protons. The solution  $u(k, r)$  is regular at the origin, i.e.,

$$u(k, r) \sim C_0 r^{\ell+1}, \quad r \rightarrow 0. \quad (33)$$

At large distances, where the nuclear part of the potential is zero,  $u(k, r)$  satisfies the asymptotic radial equation:

$$\frac{d^2 u(k, r)}{dr^2} = \left( \frac{\ell(\ell + 1)}{r^2} + \frac{2\eta k}{r} - k^2 \right) u(k, r), \quad (34)$$

whose solutions are the regular and irregular Coulomb functions  $F_l(kr, \eta)$  and  $G_l(kr, \eta)$ , respectively, and  $\eta = \frac{mZ}{k\hbar^2}$  is the Sommerfeld parameter. The outgoing and incoming Coulomb waves are usually denoted as  $H_{\ell\eta}^{\pm} = G_l(kr, \eta) \pm iF_l(kr, \eta)$ . For neutrons,  $\eta = 0$  and the asymptotic solutions are the Hankel functions. The boundary condition at  $r \geq R$  can be written as

$$u(k, r) \sim C_+ H_{\ell\eta}^+(kr), \quad r \geq R \text{ (resonant states)}, \quad (35)$$

$$u(k, r) \sim C_+ H_{\ell\eta}^+(kr) + C_- H_{\ell\eta}^-(kr), \quad r \geq R \text{ (scattering states)}, \quad (36)$$

where  $C_0, C_+$ , and  $C_-$  are normalization constants. For the resonant states, i.e., the  $S$ -matrix poles, the wave functions have a purely outgoing character; they form a discrete component of the Berggren ensemble.

In most applications, Gamow states are expressed in the coordinate representation; they are found by direct integration of the Schrödinger equation with outgoing boundary conditions. This procedure is straightforward for spherical local potentials and can be applied to deformed potentials by using a coupled-channel decomposition of the wave function [112]. In some cases, however, it is useful to work with Gamow states in momentum representation [63, 64]. The continuum discretization in  $k$ -space can be carried out using the Fourier-Bessel transform. The Schrödinger equation in momentum representation reads:

$$\frac{\hbar^2 k^2}{2m} u(k) + \int_0^{+\infty} V(k, k') u(k') dk' = \tilde{E} u(k), \quad (37)$$

where  $V(k, k')$  is the Fourier-Bessel transform of the generating potential. Contrary to the coordinate representation, where non-local potentials have to be treated with the equivalent potential method [137], local and non-local potentials are treated on the same footing in the momentum representation. Moreover, discretization of the Schrödinger equation can be replaced by matrix diagonalization [138]. Recent applications of the momentum representation can be found in Refs. [139, 93]. This way of generating of Gamow states turned out to be very effective, especially for well-deformed nuclei.

## 4.2 Normalization of single-particle states

The s.p. states in (30) need to be properly normalized, either to unity (resonant states) or to Dirac delta (scattering states).

The normalization to the Dirac delta is straightforward to achieve, as it is equivalent to the condition  $2\pi C_+ C_- = 1$  in Eq. (36), which comes from the asymptotic form of Hankel/Coulomb wave functions. The values of the constants  $C_+$  and  $C_-$  can be obtained from the matching condition at  $r = R$ :

$$\frac{d}{dr} \left[ C_+ H_{\ell\eta}^+(kR) + C_- H_{\ell\eta}^-(kR) \right] = \frac{d}{dr} u(k, R), \quad (38)$$

where  $u(k, R)$  is determined by the direct integration from  $r = 0$  to  $r = R$ .

The normalization of decaying states is, however, more complicated as, contrary to bound states, they diverge in modulus for  $r \rightarrow +\infty$ . A solution to this problem can be obtained by considering the analytic property of the norm of  $u(k, r)$ , denoted as  $\mathcal{N}(k)$ . If  $k$  is positive imaginary, i.e., the state  $u(k, r)$  is bound,  $\mathcal{N}(k)$  is given by

$$\mathcal{N}(k) = \sqrt{\int_0^{+\infty} u(k, r)^2 dr}. \quad (39)$$

For resonant states with a nonzero real part, the exterior complex scaling described in Sec. 3 can be used:

$$\begin{aligned} \int_0^{+\infty} u(k, r)^2 dr &= \int_0^R u(k, r)^2 dr + C_+^2 \int_R^{+\infty} H_{\ell\eta}^+(kr)^2 dr \\ &= \int_0^R u(k, r)^2 dr + C_+^2 \int_0^{+\infty} H_{\ell\eta}^+(kR + kxe^{i\theta})^2 e^{i\theta} dx, \end{aligned} \quad (40)$$

where  $0 < \theta < \frac{\pi}{2}$  is the angle of complex rotation. Analyticity of  $u(k, r)$  with respect to  $r$  implies that the integral (40) is independent of  $R$  and  $\theta$ . Indeed, if  $u(k, r)$  is a decaying state, there always exists a minimal angle  $\theta_c > 0$  for which the complex integral of Eq. (40) converges for  $\theta > \theta_c$ , to a value independent of  $R$  and  $\theta$ . Hence, one can define the analytic continuation of  $\mathcal{N}(k)$  as the square root of Eq. (40).

The normalized s.p. wave function  $\psi(k, \mathbf{r})$  becomes:

$$\psi(k, \mathbf{r}) = \frac{u(k, r)}{r} [Y_\ell(\hat{r}) \chi_s]_{jm}. \quad (41)$$

All the angular momentum/isospin algebra of the GSM is carried out exactly in the same way as in the standard SM. The difficulties inherent to the Berggren basis are all contained in the radial wave function  $u(k, r)$ .



### 4.3 Discretization of the scattering contour

In practical applications, as the s.p. basis must be finite, the contour integral along  $L^+$  is limited to the finite range  $k < k_{max}$  and then discretized according to a preferred quadrature. The momentum cut-off  $k_{max}$  must be sufficiently large to provide convergence. The resulting *discretized completeness relation* reads:

$$\sum_{n \in (b,d)} |u_n\rangle\langle u_n| + \int_{L^+} |u(k)\rangle\langle u(k)| dk \simeq \sum_{n \in (b,d)} |u_n\rangle\langle u_n| + \sum_i \omega_i |u(k_i)\rangle\langle u(k_i)| = \sum_i |u_i\rangle\langle u_i|, \quad (42)$$

where  $(k_i, \omega_i)$  is the set of discretized momenta and associated weights provided by a quadrature (usually, a Gauss-Legendre quadrature is chosen). The discretized scattering states

$$u_i(r) = \sqrt{\omega_i} u(k_i, r) \quad (43)$$

are normalized to unity as the discretization implies the replacement of  $\delta(k_i - k_{i'})$  by  $\omega_i \delta_{ii'}$ . The relation (42) involves both resonant and discretized scattering states; it is formally identical to the standard completeness relation in a discrete basis.

### 4.4 Gamow Hartree-Fock potential

The nature of s.p. resonant states entering the Berggren ensemble changes with the depth of the generating potential. Obviously, a broad resonant state becomes progressively narrow and eventually bound as the potential's depth increases. This implies that, in order to optimize the s.p. basis, the generating potential should be chosen according to the nucleus studied. Let us consider an example of the He chain, treated in a  $^4\text{He}$  core+valence particle framework, discussed later in this paper. The potential simulating the  $^4\text{He}$  core is fitted to reproduce the s.p. resonances in  $^5\text{He}$ . While the resulting basis will work well for a two-neutron halo nucleus  $^6\text{He}$ , it is not well suited for a four-neutron halo system  $^8\text{He}$ .

An optimal generating potential can be obtained by means of the HF method from the underlying many-body Hamiltonian. However, in order to be used in the completeness relation (6), the HF potential has to be spherical and the HF approach has to be extended to unbound systems. This approximation is referred to as the Gamow Hartree-Fock (GHF) [53]. The starting point of GHF is a GSM Hamiltonian

$$H_{GSM} = \sum_i \hat{h}_i + \sum_{i < j} \hat{V}_{ij}, \quad (44)$$

consisting of a one-body term

$$\hat{h} = \frac{\hat{p}^2}{2m} + U(r) \quad (45)$$

and a residual two-body interaction  $\hat{V}_{ij}$  acting among valence particles. The one-body field  $U(r)$  in Eq. (45) represents the core-valence interaction. It can be taken in a WS form (31). In order to impose spherical symmetry, a uniform-filling approximation can be employed, in which nucleons occupy uniformly the valence shell (i.e., no individual HF orbitals are blocked). The matrix elements of the HF potential  $U_{uf}$  between two spherical states  $\alpha$  and  $\beta$  carrying quantum numbers  $(\ell, j)$  are:

$$\langle \alpha | \hat{U}_{uf} | \beta \rangle = \langle \alpha | \hat{h} | \beta \rangle + \frac{1}{2j+1} \sum_{m, \lambda, m_\lambda} \frac{N(\lambda)}{2j_\lambda + 1} \langle \alpha m \lambda m_\lambda | \hat{V} | \beta m \lambda m_\lambda \rangle, \quad (46)$$

where  $\lambda$  is an occupied shell having quantum numbers  $(\ell_\lambda, j_\lambda)$ ,  $N(\lambda)$  is the number of particles occupying the  $\lambda$ -shell, and  $m, m_\lambda$  run over all possible values. One recalls that  $U_{uf}$  provides the exact HF potential only for closed-shell nuclei, with which all 1p-1h excitations from the GHF ground state vanish.

If the nucleus has only one particle or hole outside closed shells, it is possible to define a better approximation to  $U_{uf}$ , which has been called  $M$ -potential in Ref. [53] and is denoted as  $U_M$ . In this case, one blocks the last particle or hole in the one-body state of largest angular projection  $m$ , so that the HF ground state is coupled to

$J=m$ . The spherical  $M$ -potential is defined by averaging the HF potential over the magnetic quantum number  $m$ :

$$\langle \alpha | \hat{U}_M | \beta \rangle = \langle \alpha | \hat{h} | \beta \rangle + \frac{1}{N_{\ell j}} \sum_{m=j+1-N_{\ell j}}^j \sum_{\lambda, m_\lambda} \langle \alpha m \lambda m_\lambda | \hat{V} | \beta m \lambda m_\lambda \rangle, \quad (47)$$

where  $N_{\ell j}$  is the number of nucleons occupying the valence shell  $(\ell, j)$ . It is straightforward to show that all 1p-1h excitations from the GHF ground state involving the particle in the unfilled shell vanish in this case. While this does not hold for the hole states, one can still expect the  $M$ -potential to perform better than  $U_{uf}$  in this case.

If the HF ground state is unbound, one is forced to disregard the imaginary part of the GHF potential. For the case of one valence particle, the imaginary component of the GHF potential disappears due to antisymmetrization, and the imaginary part generated by the core shells must be spurious, as the core is assumed to be well bound. Even though a removal of an imaginary part of the HF potential slightly affects self-consistency, solutions for unbound nuclei can easily be obtained. Other aspects of the GHF procedure remain unchanged as compared to the standard HF procedure for bound systems.

Within the mean-field theory, pairing correlations can be included by means of the Hartree-Fock-Bogoliubov method (HFB). Its resonant-state extension is called Gamow-HFB [140]. For a bound nucleus, upper and lower components of one-quasi-particle Gamow states meet outgoing boundary conditions [140, 141]. While the Gamow-HFB approach allows for the study of the structure of resonant states in weakly bound paired systems, its extension to unbound nuclei still needs to be worked out, even though an approximate scheme has been devised in Ref. [142].

Another complex-energy, self-consistent approach that can be used to study particle unstable nuclei is the complex-scaled HF (CSHF) method [129]. In this approach, the HF potential is complex-rotated (27) in order to have all its occupied states square-integrable. Contrary to GHF, self-consistency is fully maintained for unbound nuclei, because the CSHF potential is complex. However, one cannot extend CSHF beyond the HF level. For that, scattering states would have to be calculated in all directions of the complex energy plane in order to extend CS to non-resonant continuum. This is impossible because the CSHF potential diverges exponentially in some regions of the complex plane. Consequently, as CSHF cannot be used to generate a GSM basis, and pairing correlations cannot be treated within CS-HFB, the range of applications of CSHF is rather limited.

## 4.5 Numerical tests of the Berggren completeness relation

In this Section, we illustrate the validity and accuracy of Eq. (6) by means of several numerical examples. To this end, we consider the expansion of resonant states generated by a WS potential  $V_E(r)$  (31) with a Berggren basis generated by a WS potential  $V_B(r)$  of different  $V_0$  strength, but identical for all remaining parameters. The s.p. Hamiltonian to be diagonalized  $\hat{h}_E$  is represented by a continuous matrix in the eigenstates of  $\hat{h}_B = \frac{\hat{p}^2}{2m} + V_B$ :

$$\begin{aligned} \langle u_n | \frac{\hat{p}^2}{2m} + V_E | u_p \rangle &= \frac{\hbar^2 k_n^2}{2m} \delta_{np} + \int_0^{+\infty} u_n(r) \Delta(r) u_p(r) dr, \\ \langle u(k) | \frac{\hat{p}^2}{2m} + V_E | u(k') \rangle &= \frac{\hbar^2 k^2}{2m} \delta(k - k') + \int_0^{+\infty} u(k, r) \Delta(r) u(k', r) dr, \\ \langle u_n | \frac{\hat{p}^2}{2m} + V_E | u(k) \rangle &= \int_0^{+\infty} u_n(r) \Delta(r) u(k, r) dr, \end{aligned} \quad (48)$$

where  $u_i(r)$  and  $u(k, r)$  are, respectively, resonant and scattering states of the Berggren basis generated by  $\hat{h}_B$ , and  $\Delta(r) \equiv V_E(r) - V_B(r)$ .

Following the contour discretization described in Sec. 4.3, the continuous representation of (48) is approximated by a complex symmetric matrix:

$$\langle u_i | \frac{\hat{p}^2}{2m} + V_E | u_{i'} \rangle = \frac{\hbar^2 k_i^2}{2m} \delta_{ii'} + \int_0^{+\infty} u_i(r) \Delta(r) u_{i'}(r) dr, \quad (49)$$

where  $u_i(r)$  are discrete vectors representing both resonant and scattering states. The eigenvectors of (49) represent the resonant and discretized scattering states of  $V_E$ .

As an illustrative example, let us consider the expansion of a neutron  $2p_{3/2}$  eigenstate of a WS potential (31) in a Berggren basis. The radial wave function of the expanded state, denoted as  $u_E(r)$ , is a linear combination of  $p_{3/2}$  basis states  $u_B(k, r)$ :

$$u_E(r) = \sum_{n \in (b,d)} c_n u_B(k_n, r) + \int_{L^+} c(k) u_B(k, r) dk, \quad (50)$$

where  $c_n$  and  $c(k)$  are the expansion coefficients. As discussed in Sec. 4.3,  $L^+$  has to be discretized.

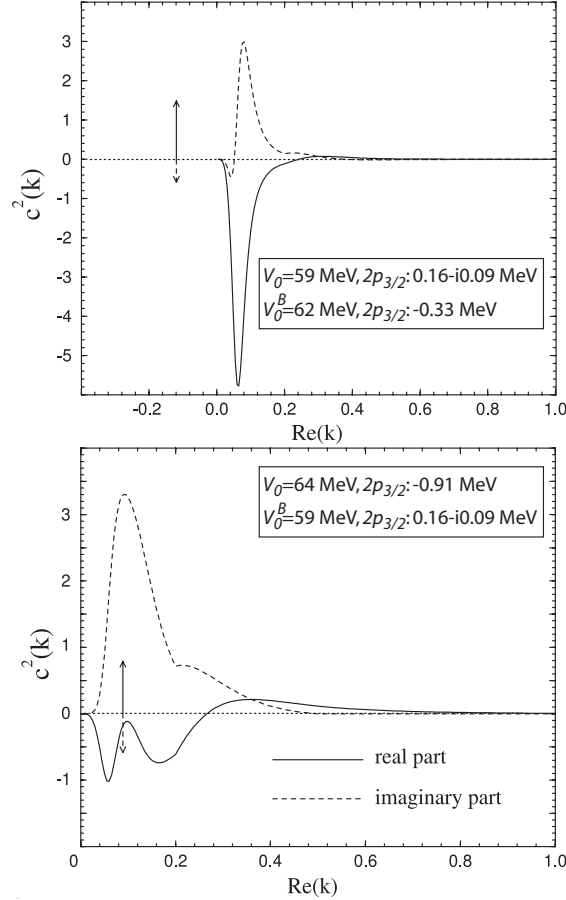


Figure 5: Distribution of the squared amplitudes  $c^2(k)$  of the neutron state  $2p_{3/2}$  of the WS in the basis generated by another WS potential. The amplitudes of both real (solid line) and imaginary (dashed line) parts of the wave function are plotted as a function of  $\text{Re}[k]$ . The height of the arrow gives the squared amplitude of the  $2p_{3/2}$  resonant state contained in the basis. The complex contour  $L^+$  corresponds to three straight segments in the complex  $k$ -plane, joining the points:  $k_0=0.0-i0.0$ ,  $k_1=0.2-i0.2$ ,  $k_2=0.5-i0.0$ , and  $k_3=2.0-i0.0$ , all in units of  $\text{fm}^{-1}$ . Top:  $V_0=59$  MeV,  $V_0^{(B)}=62$  MeV. Here the expanded state is a  $2p_{3/2}$  resonance. Bottom:  $V_0=64$  MeV,  $V_0^{(B)}=59$  MeV. Here the expanded state is bound. (Example taken from Ref. [119] where details of the calculation can be found.)

The expansion coefficients (50) are shown in Fig. 5 where the depth of the WS potential is varied to generate a resonant or bound  $2p_{3/2}$  state. In both cases, the importance of the scattering continuum is noticeable. This example nicely demonstrates the invalidity of the pole approximation to provide a quantitative description of weakly bound or resonant states.

More examples of s.p. expansions can be found in Refs. [119] (neutrons) and [53] (protons). Let us only mention that in the proton case the role of the scattering continuum is somehow reduced due to the confining

effect of the Coulomb barrier, especially at small energies. Still, for a precise description of eigenstates, the scattering component needs to be included.

## 5 Gamow Shell Model

### 5.1 Many-body GSM basis

The discretized basis (42) can be used to extend the completeness relation to the many-body case, in a full analogy with the standard SM in a complete discrete basis, e.g., the HO basis. The many-body basis of GSM corresponds to Slater determinants (SD) built from one-body states constituting the Berggren ensemble:

$$|SD\rangle_n = |u_{i_1} \cdots u_{i_A}\rangle, \quad (51)$$

where  $|u_i\rangle$  are properly normalized one-body states (either resonant or scattering) of a generating potential. The completeness of the Berggren ensemble guarantees the closure relation for the many-body GSM basis:

$$\sum_n |SD_n\rangle\langle SD_n| \sim 1, \quad (52)$$

where  $n$  runs over all possible SDs (51). The approximate equality in (52) is a consequence of the continuum discretization.

### 5.2 Determination of many-body resonant states

The GSM Hamiltonian matrix in the basis (52) is complex symmetric. In a standard SM, the Lanczos method is often used to determine the eigenstates of the Hamiltonian matrix. It allows calculating selected states, e.g., ground state and low-lying excited states, in very large configuration spaces. However, the Lanczos method cannot be applied *mutatis mutandis* to the GSM matrix problem, due to the presence of scattering states. As many-body resonant states are embedded in the discretized continuum of many-body scattering states, the lowest-energy principle cannot be used to guide our choice.

One way of selecting many-body resonant states was proposed in Refs. [117, 143] dealing with systems having two valence nucleons. Here, the selection of two-particle resonances is done with a suitable choice of the contour  $L^+$ . It was realized that by choosing a square-shaped contour, the resonant states appear in the so-called allowed region of the complex-energy plane [117] and this facilitates their identification.

In Fig. 6 the allowed region is a square-shaped area defined by a s.p. contour. Due to the low density of two-particle scattering states in this region, the trajectories of two-particle resonances can be easily followed as the strength of the residual interaction increases. It has been observed that the two-body resonant states are mostly based on the pole-pole (p-p) configuration, although the role of discretized continuum states (p-c, c-c) in Fig. 6 is not negligible. The result that the correlated two-particle resonant states are built mainly from configurations formed from s.p. resonant states gives strong support for the use of the overlap method discussed below. Unfortunately this convenient method might not be generalized easily to the case of more than two valence particles.

Another solution to the problem of resonant-state selection, particularly useful in the case of several valence nucleons, has been proposed in Ref. [119]. It is based on the overlap method, utilizing the property that the main components of many-body resonant states are built from resonant SD. In the first step, the GSM Hamiltonian is diagonalized in a smaller basis consisting of s.p. resonant states only (a pole approximation). Here, some variant of the Lanczos method can be applied. The diagonalization yields the first-order approximation to many-body resonances  $|\Psi_0\rangle$ . In the second step,  $|\Psi_0\rangle$  is used as a Lanczos pivot. Diagonalization of the GSM Hamiltonian in this subspace yields many-body eigenstates. The resonant state is the eigenstate  $|\Psi\rangle$  which maximizes the overlap  $|\langle\Psi_0|\Psi\rangle|$ . This method identifies the many-body resonant state provided its coupling to the non-resonant continuum is weak, i.e. 10-30%. This condition is usually satisfied, especially if the one-body basis has been optimized by way of the GHF procedure.

Fig. 7 illustrates the overlap technique for  $J^\pi = 0^+$  states in  $^{20}\text{O}$  considered as a four-neutron system outside the  $^{16}\text{O}$  core [119]. Diagonalization of the GSM Hamiltonian matrix provides complex-energy eigenstates.

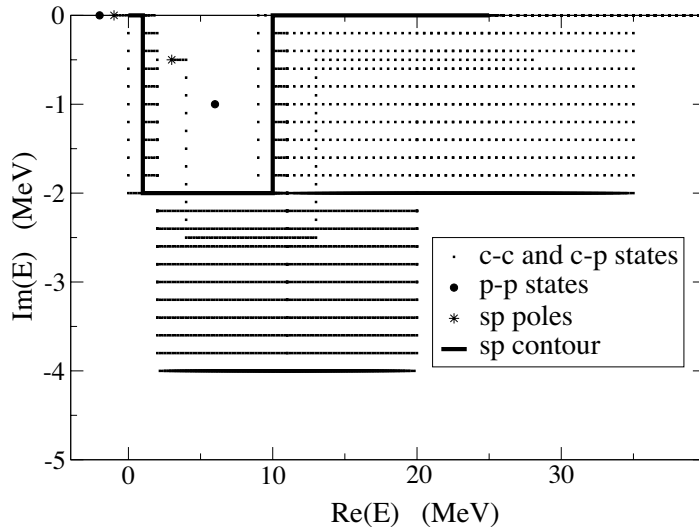


Figure 6: A typical square-shaped contour in the complex energy-plane used for calculation of two particle resonant states in Ref. [117]. Stars mark the s.p. pole (p) states, while the thick line denotes the scattering contour (c). Full dots denote the two-particle energies of the pole-pole type and those in which at least one single particle is in a scattering state. (See Ref. [117] for details.)

Compared with Fig. 6, the number of many-body states is much larger and the regular pattern of non-resonant states reflecting the structure of the scattering contour is gone (the figure represents the projection of four-dimensional trajectories onto two dimensional space). While the two lowest (bound) states can be simply identified by inspection, for the higher-lying states it is practically impossible to separate the resonances from the non-resonant continuum. However, the procedure outlined above makes it possible to identify unambiguously the many-body resonance states. It is seen that the resonant states shown in Fig. 7 they all have negligible or very small positive widths, as expected. The many-body resonant states appear to be stable with respect to small changes of the contour (as the physical solutions should not be dependent on the deformation of the basis). On the other hand, the states representing the non-resonant many-body continuum move in the complex energy plane with the contour's deformation.

### 5.3 GSM Hamiltonian

Hamiltonian matrix elements between resonant states can be calculated with complex scaling (see Sec. 3). However, this is not the case with scattering states, for which complex-scaled integrals may not converge regardless of the angle of rotation, as is the case for the normalization of scattering states (see Sec. 4.2). In the latter situation, since the result is analytical (Dirac delta), the problem can be dealt with by means of the contour discretization (see Sec. 4.3). However, it is very difficult to calculate matrix elements of general interactions; hence, in the first applications, only localized Hamiltonians were used. Examples are the Gaussian separable interaction [117, 139], the Surface Delta interaction [118, 119], and the Surface Gaussian interaction (SGI) [53] (see Sec. 6.1). For these schematic forces, the calculation of two-body matrix elements is straightforward. In order to deal with realistic interactions, which are very complicated to express and infinite-ranged in shell-model coordinates, a new approach, based on a HO basis expansion technique, had to be devised (see Sec. 6.2).

### 5.4 Matrix elements of electromagnetic operators

In the GSM, the electromagnetic (EM) transition selection rules and the angular momentum and isospin algebra do not change compared to the standard SM. However, to calculate the EM transitions, one can no longer use the long wavelength approximation because of the presence of the non resonant continuum. Indeed, for the diagonal EM matrix elements  $\langle n_i \ell_i j_i k_i | O | n_f \ell_f j_f k_f \rangle$  ( $k_i = k_f$ ) between the scattering states, the complex scaling cannot be carried out. Furthermore, one cannot employ the long wavelength approximation to the

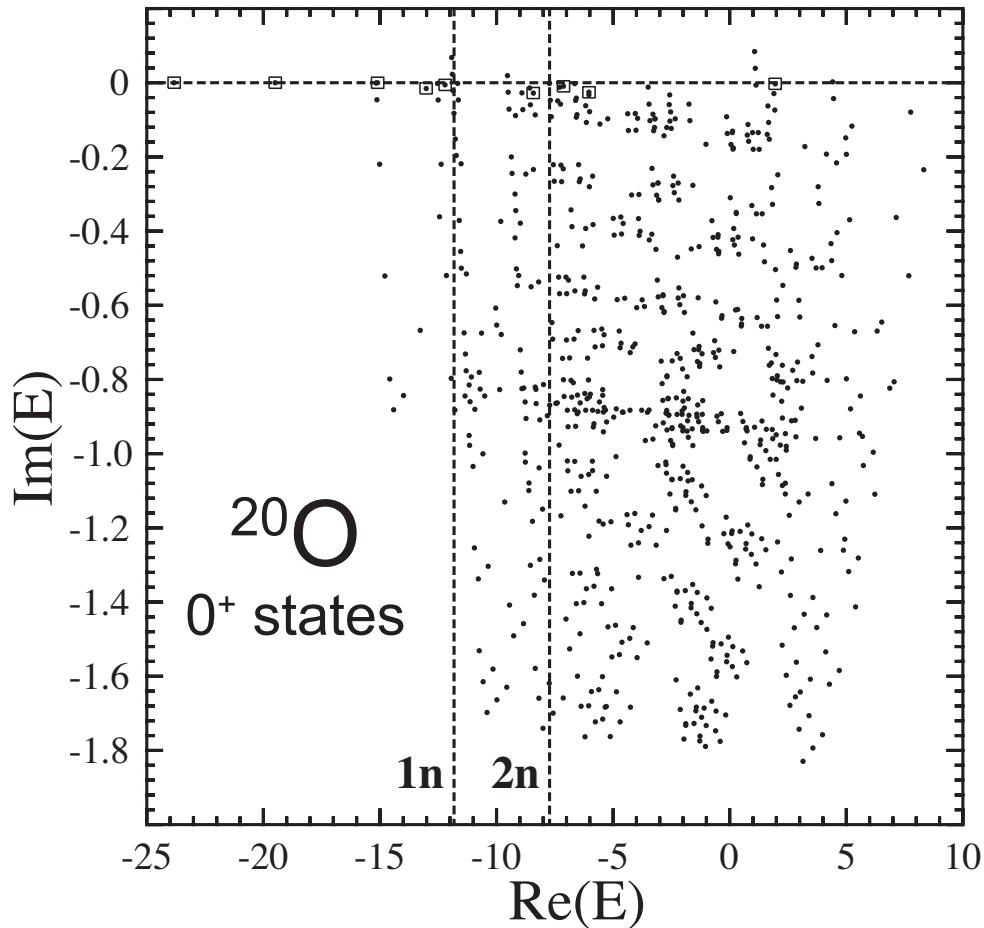


Figure 7: Complex energies of the  $0^+$  states in  $^{20}\text{O}$  calculated in the GSM+SDI model. One- (1n) and two-neutron (2n) emission thresholds are indicated. The many-body resonant states (bound states and narrow resonances) are marked by squares. Note that all those state have zero or positive widths, as expected. The remaining eigenstates represent the non-resonant continuum.

EM operators as they behave like  $r^\lambda$ . Without the long wavelength approximation, however, the continuum-continuum matrix elements become finite, because it is always possible to carry out a complex scaling with the Bessel function of the photon  $j_L(qr)$ , as  $q \neq 0$ . As all the other matrix elements can be regularized, the EM matrix elements are all well defined.

## 5.5 Optimization of the scattering contour of GSM using the Density Matrix Renormalization Group method

The application of the Berggren ensemble to GSM is associated with the explosive growth in the number of configurations with the number of active particles and the size of the s.p. space. To ensure completeness of the Berggren basis, for each resonant s.p. state  $(\ell, j)$ , one should include a large number of s.p. scattering states  $\{(\ell, j)^{(f)}; f = 1, \dots, M\}_c$  lying on a discretized contour  $L_+^{\ell j}$ . All these states become new active shells; hence, the configuration space of GSM grows extremely fast with the number of contour discretization points. Moreover, the resulting complex-symmetric GSM Hamiltonian matrix is significantly denser than the Hamiltonian matrix of a conventional SM. Hence, taming the dimensionality growth in solving the many-body Schrödinger equation is crucial.

There are several specific features of the *dimensional catastrophe* in GSM that may facilitate this task. Firstly, of all GSM eigenstates, of major interest are the many-body resonant states. As discussed in Sec. 5.2, these eigenstates represent a narrow class of spatially localized states, immersed in a sea of non-resonant scattering states. Eigenstates of the GSM Hamiltonian in the pole space can serve as the reference vectors,

helping to identify resonant eigenstates out of a huge space of all GSM eigenvectors. Hence, instead of a direct diagonalization of the GSM Hamiltonian matrix, a strategy should be developed for an optimization of the scattering space.

The Density Matrix Renormalization Group (DMRG) method was introduced in Ref. [144] to overcome the limitations of Wilson-type renormalization groups to describe strongly correlated 1D lattice systems with short-range interactions (see also recent reviews [145, 146]). Up to now, most of the DMRG studies were focused on equilibrium properties in strongly correlated closed quantum systems (CQS) with a Hermitian density matrix. Nevertheless, non-equilibrium systems involving non-Hermitian and non-symmetric density matrices can also be treated in the DMRG [147]. The DMRG approach is ideally suited to optimize the size of the scattering space in the GSM problem as the properties of the non-resonant shells vary smoothly along the scattering contour. The main idea of the GSM+DMRG truncation algorithm [148, 149] is to gradually consider different s.p. shells of the discretized non-resonant continuum in the configuration space and retain only  $N_{\text{opt}}$  optimal states dictated by the eigenvalues of the density matrix with the largest modulus. Since the GSM Hamiltonian is complex symmetric, it is the complex (or generalized) variational principle [150, 151, 152] than the usual variational principle that governs the GSM+DMRG algorithm [149].

The iterative GSM+DMRG procedure of constructing the eigenvectors is divided into two phases: the warm-up phase and the sweeping phase. There are two essential conditions which guarantee that the GSM+DMRG method yields correct results. The first one is to ensure that all possible couplings in the many-body wave function, allowed by the symmetries of the problem, are present in the warm-up phase. This means that one should keep all the essential partial waves which are present in DMRG wave functions, even though they may be absent at the pole approximation level. The second condition is to ensure that the reference state  $|\Psi_J\rangle^{(0)}$ , which is a key ingredient in selecting the target state  $|\Psi_J\rangle$  from the set of all GSM solutions of a given angular momentum and parity at each iteration step, is correctly described.

The DMRG configuration space can be initially divided into two subspaces:  $A$  (the reference subspace built from all s.p. resonant shells  $\{(n_1, \ell_1, j_1), (n_2, \ell_2, j_2), \dots\}$  and one representative non-resonant shell for each remaining partial wave  $\{(\ell_p, j_p), (\ell_r, j_r), \dots\}$  in the valence space) that is essential to produce many-body couplings, and  $B$  (the complementary subspace built from the s.p. non-resonant shells  $\{(\ell_1, j_1)\}_c, \{(\ell_2, j_2)\}_c, \dots\}$ ). One begins in the warm-up phase by constructing all product states  $|k\rangle_A$  forming the reference subspace  $A$ .

The many-body configurations in  $A$  can be classified in different families  $\{n; j_A\}$  according to their number of nucleons  $n$  and total angular momentum  $j_A$ . All possible matrix elements of sub-operators of the two-body Hamiltonian acting in  $A$  are calculated and stored. The Hamiltonian is then diagonalized in  $A$  to provide the zeroth-order approximation to the targeted eigenstate  $|J^\pi\rangle$ , called the reference state  $|\Psi_J\rangle^{(0)}$ . In the next step, the subspace of the first scattering shell  $(\ell, j)_1$  belonging to the discretized contour  $L^+$  is added. Within this shell, one constructs all possible many-body states, denoted as  $|i\rangle_B$  and grouped in  $\{n_B; j_B\}$  families, and all matrix elements of sub-operators of the Hamiltonian. This ensemble serves as a basis in which the GSM Hamiltonian is diagonalized. The target state  $|\Psi_J\rangle$  is selected among the eigenstates of the Hamiltonian as the one having the largest overlap with the reference vector  $|\Psi_J\rangle^{(0)}$ . Based on the expansion:

$$|\Psi_J\rangle = \sum_{k_A, i_B} c_{i_B(j_B)}^{k_A(j_A)} \{|k_A(j_A)\rangle \otimes |i_B(j_B)\rangle\}^J, \quad (53)$$

by summing over the reference subspace  $A$  for a fixed value of  $j_B$ , one obtains the reduced density matrix [153]:

$$\rho_{i_B' i_B}^B(n_B, j_B) \equiv \sum_{k_A} c_{i_B(j_B)}^{k_A(j_A)} c_{i_B'(j_B)}^{k_A(j_A)} \quad (54)$$

which is complex-symmetric in the metric defining the Berggren ensemble. In the warm-up phase, the reference subspace becomes the ‘medium’ for the ‘system’ part in the  $B$  subspace.

Truncation in the system part is dictated by the density matrix. The reduced density matrix is diagonalized and one retains at most  $N_{\text{opt}}$  eigenstates of  $\hat{\rho}^B$ :

$$\hat{\rho}^B(n_B, j_B)|\alpha\rangle_B = w_\alpha|\alpha\rangle_B \quad (55)$$

having the largest nonzero values of  $|w_\alpha|$ . Then, one expresses the eigenstates  $|\alpha\rangle_B$  in terms of the vectors  $|i\rangle_B$  in  $B$ :

$$|\alpha\rangle_B = \sum_i d_i^\alpha |i\rangle_B \quad (56)$$

and all matrix elements of the sub-operators in these optimized states,

$${}_B\langle\alpha|O|\beta\rangle_B = \sum_{i,i'} d_i^\alpha d_{i'}^\beta {}_B\langle i|O|i'\rangle_B \quad (57)$$

are recalculated and stored. In a similar way, the warm-up procedure continues by adding to the system part the configurations containing particles in the next scattering shells until the last shell in  $B$  is reached. At this point, all s.p. states have been considered, the warm-up phase ends, and the sweeping phase begins (cf. Refs. [148, 149] for details). The sequence of sweep-up and sweep-down phases continues until convergence for target eigenvalues is achieved.

It has been demonstrated [148, 149] that the fully converged GSM results, with respect to both the number of sweeps and the number of shells in the discretized continua, can be obtained using the GSM+DMRG algorithm. Several attractive features have been found. Firstly, the rank  $d_H^{\max}$  of the biggest reduced density matrix to be diagonalized in GSM+DMRG is practically constant with respect to the number of shells  $N_{\text{sh}}$ . Hence, the ratio  $d_H^{\max}/D$ , where  $D$  is the dimension of the GSM Hamiltonian matrix, decreases rapidly [148]. Secondly, the converged complex eigenenergies depend weakly on the number of vectors at each step of the iteration procedure, and the uncertainty of calculated eigenenergies weakly depends on  $N_{\text{sh}}$ . This means that the convergence features of the GSM+DMRG procedure can be tested by varying  $N_{\text{sh}}$  and  $N_{\text{opt}}$ . Once those parameters are optimized in ‘small-scale’ GSM+DMRG calculations, the final calculations can be performed in the large model space to obtain fully converged results. Thirdly, the GSM+DMRG energy averaged over one sweep exhibits excellent exponential convergence with  $N_{\text{opt}}$ , which allows to deduce the asymptotic value with good precision. These encouraging features of the GSM+DMRG algorithm open the possibility for systematic and high-precision studies of complex, weakly bound, or unbound nuclei, which require large configuration spaces for their correct description.

## 6 GSM applications

### 6.1 GSM applications with schematic Hamiltonians

In the first applications of GSM, schematic core+valence Hamiltonians were applied. In Ref. [119], neutron-rich isotopes of He and O have been studied by approximating the residual interaction in (44) with the Surface Delta Interaction (SDI):

$$V(\mathbf{r}_i, \mathbf{r}_j) = -V_{SDI} \delta(r_i - R_0) \delta(r_j - R_0), \quad (58)$$

where  $r_i = |\mathbf{r}_i|$ ,  $R_0$  is the radius of the WS core potential, and  $V_{SDI}$  is the SDI strength. The main advantage of the zero-range SDI interaction is that its two-body matrix elements can be easily calculated and no complex scaling is involved. In the He case, the Berggren basis consisted of  $0p_{3/2}$  and  $0p_{1/2}$  resonant states and the associated scattering continua  $p_{3/2}$  and  $p_{1/2}$ . For the O isotopes, valence space consisted of the bound  $0d_{5/2}$ ,  $1s_{1/2}$  states, the  $0d_{3/2}$  resonance, and the  $d_{3/2}$  scattering contour. Since other scattering channels can only impact real energies, they were not included as they could effectively be taken into account by renormalizing the SDI interaction strength. Results for the chain of oxygen isotopes are shown in Fig. 8.

An early example of spectroscopic studies with GSM is shown in Fig. 9 which displays the level scheme of  $^{19}\text{O}$  calculated with GSM+SDI. The main experimental features are reproduced. In addition to energy levels, calculations were carried out for electromagnetic  $E2$  and  $M1$  transition probabilities.

The GHF technique of basis optimization cannot be used effectively with SDI. Hence, in order to improve convergence of results, it was necessary to employ another interaction. For that, a delta component of the SDI interaction was replaced with a Gaussian form factor, thereby providing finite-range, while the second delta



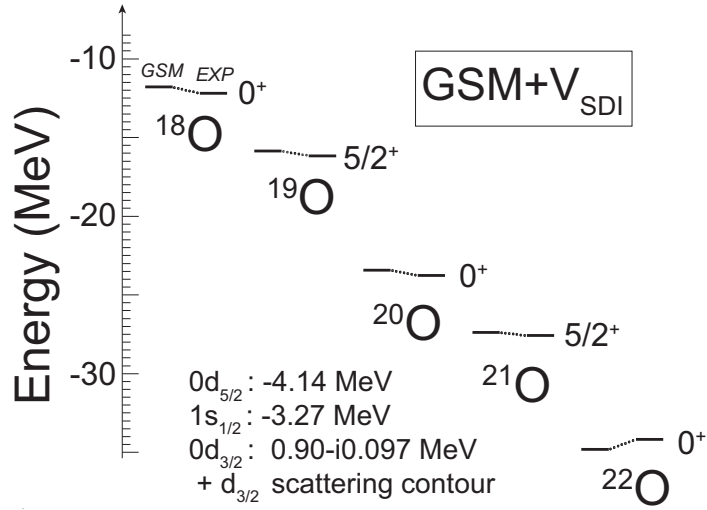


Figure 8: Experimental (EXP) and predicted (GSM+ $V_{SDI}$ ) [119] binding energies of  $^{18-22}\text{O}$ . The energies are given with respect to the  $^{16}\text{O}$  core.

function remains in order to keep the interaction surface-peaked. The resulting surface Gaussian interaction (SGI) reads:

$$V(\mathbf{r}_i, \mathbf{r}_j) = -V_{SGI}^{(J,T)} \exp \left[ - \left( \frac{\mathbf{r}_i - \mathbf{r}_j}{\mu} \right)^2 \right] \delta(r_i + r_j - 2R_0), \quad (59)$$

where  $\mu$  is the range,  $V_{SGI}^{(J)}$  is the strength in the  $JT$  channel, and all other values are defined similarly to Eq. (58). Two-body matrix elements can still be conveniently calculated with the SGI interaction, as its radial components are one-dimensional finite integrals. The fact that only one delta function appears in Eq. (59) implies that the GHF-SGI potential is well defined in coordinate space, albeit of non-local character. Non-locality of spherical potentials is conveniently treated via the equivalent potential method [53], in which a non-local potential is replaced by a local but state-dependent potential. The results of GSM-SGI calculations for the neutron-rich He isotopes are shown in Fig. 10. One obtains a reasonable description of the ground-state(g.s.) energies and excited states relative to the g.s. energy of  $^4\text{He}$ .

A similar calculation for the lithium chain [53] suggests that monopole corrections have to be added to the  $T = 0$  matrix elements of SGI, modeled through a particle number dependence of  $V_{SGI}^{(J,T=0)}$ . While experimental data for  $^6\text{Li}$  and  $^7\text{Li}$  are fairly reproduced, the drip-line nuclei  $^{10}\text{Li}$  and  $^{11}\text{Li}$  are predicted to be overbound. This is due to a rather limited configuration space used in Ref. [53]; most importantly, the neglect of  $s$ -waves. Clearly, for a qualitative description of the Borromean halo nucleus  $^{11}\text{Li}$ , an extended valence space and more realistic interactions are needed, as well as a proper treatment of the center-of-mass motion.

## 6.2 GSM with realistic interactions

The inclusion of realistic interactions in GSM has been a theoretical and practical challenge. Standard SM methods rely on the  $G$ -matrix formalism [154] and Lee-Suzuki similarity transformation [155]. The Lee-Suzuki projection operator formalism or the renormalization group technique can be used to derive low-momentum interactions, usually denoted as  $V_{low-k}$  [156]. The extension of the Lee-Suzuki formalism to the complex-energy GSM framework has been done in Ref. [139] where applications to Gaussian-type interactions can be found.

Contrary to schematic interactions used in early GSM calculations, realistic interactions have a very complicated structure [157, 158, 159]. They are defined in a center-of-mass frame, so that the transformation to the laboratory frame has to be carried out. For a HO basis, this can be done by using the Brody-Moshinsky coefficients [160]. However, the generalization of this scheme to arbitrary bases through the vector-bracket transformation [161, 162, 163] is very time consuming, as the finite sums in Moshinsky transformation must be replaced by sums of two-dimensional momentum integrals. For the multipole decomposition of the realistic



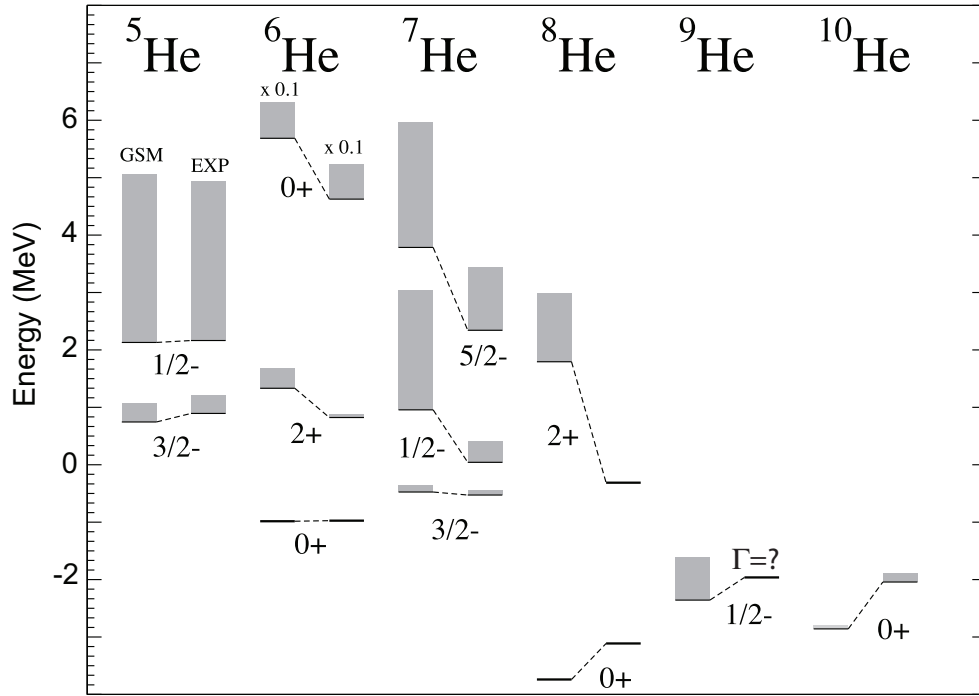


Figure 10: Experimental (EXP) and predicted (GSM) binding energies and spectra of helium isotopes obtained with the SGI Hamiltonian. The resonance widths are indicated by shading. The energies are given with respect to the core of  ${}^4\text{He}$ . The ground-state width of  ${}^9\text{He}$  is not known experimentally; hence, it is not indicated.

nuclear interaction only. Since the kinetic and Coulomb terms are treated exactly in the asymptotic zone, the new method is capable of describing weakly bound and unbound states.

$N_{\max}$	${}^6\text{He}: 0_1^+$	${}^6\text{He}: 0_2^+$	${}^{18}\text{O}: 4_2^+$
4	-0.4760 (0.0000)	0.9504 (-0.0467)	-1.4373 (-0.8275)
6	-0.4714 (0.0000)	0.9546 (-0.0461)	-1.4292 (-0.7600)
8	-0.4719 (0.0000)	0.9597 (-0.0453)	-1.4380 (-0.7405)
10	-0.4721 (0.0000)	0.9602 (-0.0452)	-1.4400 (-0.7390)
12	-0.4721 (0.0000)	0.9600 (-0.0452)	-1.4393 (-0.7401)
14	-0.4721 (0.0000)	0.9601 (-0.0452)	-1.4394 (-0.7401)
16	-0.4721 (0.0000)	0.9601 (-0.0453)	-1.4394 (-0.7401)
18	-0.4721 (0.0000)	0.9601 (-0.0453)	-1.4394 (-0.7401)
20	-0.4721 (0.0000)	0.9601 (-0.0453)	-1.4394 (-0.7401)

Table 2: Energy convergence for  $0_1^+$  and  $2_1^+$  states in  ${}^6\text{He}$  and  $4_2^+$  state in  ${}^{18}\text{O}$  versus the number  $N_{\max}$  of HO nodes in the expansion of the realistic low-momentum  $\text{N}^3\text{LO}$  nucleon-nucleon interaction. The imaginary part of the energy is shown in parentheses. A cut-off of  $1.9 \text{ fm}^{-1}$  was used for the center-of-mass momentum. The oscillator length is  $b=2 \text{ fm}$ . All energies are in MeV. (From Ref. [138].)

First applications of GSM with realistic interactions were carried out in Ref. [138] with the low-momentum potential  $V_{low-k}$  [156] for  ${}^6\text{He}$  and  ${}^{18}\text{O}$ , viewed as two-neutron systems. The  ${}^4\text{He}$  or  ${}^{16}\text{O}$  cores were approximated by a GHF potential. The same GHF potential was also used to generate the Berggren basis in  $spd$  neutron partial waves.  $V_{low-k}$  was obtained from the chiral  $\text{N}^3\text{LO}$  interaction [159] with a momentum cut-off  $\Lambda = 1.9 \text{ fm}^{-1}$ . The calculated energies of selected states in  ${}^6\text{He}$  and  ${}^{18}\text{O}$  are shown in Table 6.2 as a function of the HO states used in the expansion (60). One can see that the results are already stabilized at  $N_{\max} \sim 10$ , even for resonant states having a sizeable width. In order to show that asymptotic properties can be reliably calculated in this scheme, Fig. 11 shows the density distribution of the valence neutrons in the halo nucleus  ${}^6\text{He}$ . The

results are already reliable at  $N_{\max}=4$  while perfect convergence is attained at  $N_{\max}=10$ .

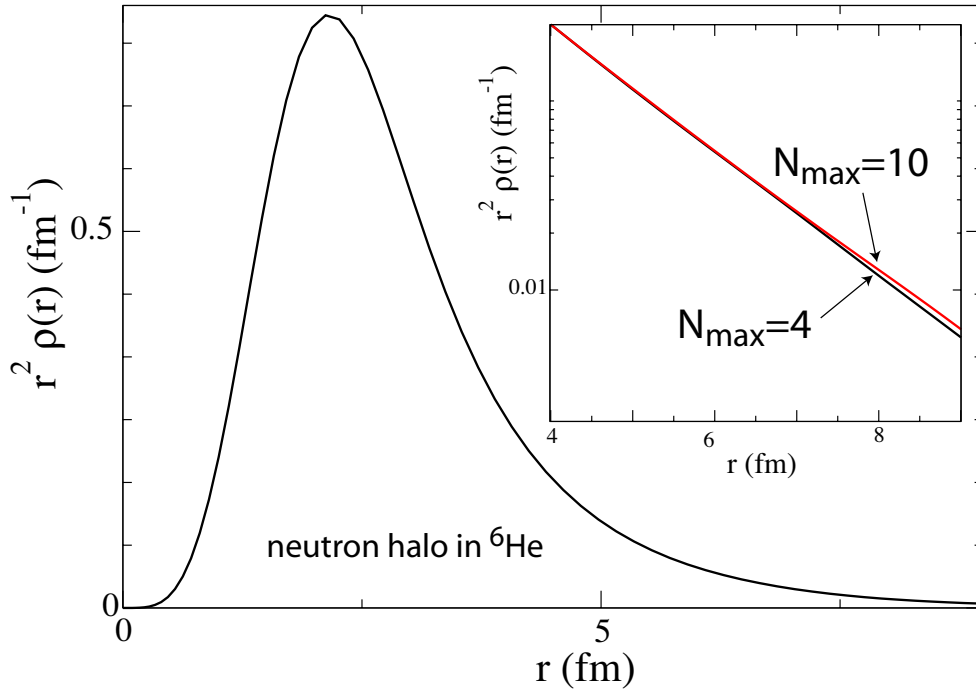


Figure 11: Neutron halo density of the ground state of  ${}^6\text{He}$  calculated in GSM+ $V_{\text{low-}k}$  [138]. The full convergence is achieved at  $N_{\max} \sim 10$ , see the inset.

In the context of *ab initio* many-body techniques, the Berggren ensemble has recently been employed in the coupled-cluster approach [164] to study neutron-rich He isotopes. This work demonstrates the usefulness of a complex-energy framework for a microscopic description of weakly bound and unbound systems.

### 6.3 Center-of-mass treatment in GSM

In SM approaches, special attention is paid to the removal of the spurious center-of-mass (CM) motion [165, 166], and GSM is no exception. The standard SM treatment of CM is based on the Lawson method [160] which, unfortunately, cannot be used within the GSM framework due to the fact that the matrix elements of  $\mathbf{R}^2$  ( $\mathbf{R}$  is the CM coordinate) cannot be regularized using the complex scaling technique. One possible solution is to replace the CM Hamiltonian by the square of the  $L_z$  component of the CM angular momentum operator  $\mathbf{L} = \mathbf{R} \times \mathbf{P}$ . Using of  $\mathbf{L}^2$  instead of  $L_z^2$ , would be equivalent but more complicated because  $\mathbf{L}^2$  is a four-body operator. In this generalized Lawson method, the CM part of SM nuclear states is not projected onto a 0s HO state, but on a  $L=0$  CM state.

Another possibility is to solve the GSM problem directly in relative coordinates. While the Jacobi coordinates have to be excluded for practical reasons, as effects due to antisymmetrization become quickly intractable when the number of coordinates increases, one can define simple CM coordinates in a core+valence framework within the cluster-orbital shell model (COSM) [167]. In COSM, all coordinates are taken with respect to the core CM, so that translational invariance is strictly preserved. With COSM coordinates being particle coordinates, Slater determinants can be easily defined within this scheme. The translationally-invariant COSM Hamiltonian can be written as:

$$H = H_c + \sum_{i=1}^{A_v} \left( \frac{p_i^2}{2m} + U_i \right) + \sum_{i<j}^{A_v} \left( \hat{V}_{ij} + \frac{\mathbf{p}_i \cdot \mathbf{p}_j}{(A_c + 1)m} \right), \quad (61)$$

where  $A_c$  and  $A_v$  is the number of core and valence particles, respectively. The principal difference between the previously introduced GSM Hamiltonian (44) and that of COSM is the term proportional to  $\mathbf{p}_i \cdot \mathbf{p}_j$  which takes into account the recoil of the active nucleons. The recoil term can be treated in the momentum representation

using the Bessel expansion method and the same  $L^+$  complex contour for all partial waves. Another possibility is to expand  $\mathbf{p}_i$  in a basis of bound states, as done for realistic interactions in Sec. 6.2.

Because the transformation from the laboratory to COSM frame is very difficult to handle [168], there are fundamental problems with using realistic interactions in a COSM framework. Nevertheless, this scheme is suitable for the development of *effective* interactions for light nuclei.

## 6.4 Overlap integrals and spectroscopic factors in GSM

Cross sections of direct reactions can be expressed as products of two factors. The first one depends on kinetic aspects of the reaction while the other one, depending on the structure of the states involved, is called the spectroscopic factor [169, 170, 171]. The experimental deduction of spectroscopic factors can sometimes be difficult due to probe- and model-dependence [172, 173, 174]. In this context, GSM is a useful tool as it provides both configuration mixing and a proper description of the particle continuum of both resonant and non-resonant character.

Spectroscopic factors are defined as the norm of the one-nucleon radial overlap integral  $u_{\ell j}(r)$  [170, 171]:

$$u_{\ell j}(r) = \langle \Psi_A^{J_A} | [ |\Psi_{A-1}^{J_{A-1}} \rangle \otimes | \ell, j \rangle ]^{J_A} \rangle, \quad (62)$$

where  $|\Psi_A^{J_A}\rangle$  and  $|\Psi_{A-1}^{J_{A-1}}\rangle$  are wave functions of nuclei  $A$  and  $A-1$  and  $|\ell, j\rangle$  is the angular-spin part of the channel function. The angular-spin degrees of freedom are integrated out in Eq. (62) so that  $u_{\ell j}$  depends only on the relative radial coordinate of the transferred particle.

Using a decomposition of the  $(\ell, j)$  channel in the complete Berggren basis  $\mathcal{B}$ , one obtains:

$$u_{\ell j}(r) = \sum_{\mathcal{B}} \langle \widetilde{\Psi}_A^{J_A} | a_{\ell j}^+(\mathcal{B}) | \Psi_{A-1}^{J_{A-1}} \rangle \langle r \ell j | \mathcal{B} \rangle, \quad (63)$$

$$S^2 = \sum_{\mathcal{B}} \langle \widetilde{\Psi}_A^{J_A} | a_{\ell j}^+(\mathcal{B}) | \Psi_{A-1}^{J_{A-1}} \rangle^2, \quad (64)$$

where  $a_{\ell j}^+(\mathcal{B})$  is a creation operator associated with a s.p. Berggren state  $|\mathcal{B}\rangle$ . Since Eqs. (63,64) involve summation over all discrete Gamow states and integration over all scattering states along the contour  $L_+^{\ell j}$ , the final result is independent of the s.p. basis assumed. This is in contrast to standard SM calculations where the model dependence of SFs enters through the specific choice of a s.p. state  $a_{n\ell j}^+$ .

Of particular interest is a non-analytic behavior of direct reaction cross section near the particle emission threshold [175, 176, 177, 178, 179]. It manifests itself by a discontinuity in the cross section and/or of its derivatives (the so-called Wigner cusp); it often arises from a redistribution of particle flux when a new reaction channel opens. This phenomenon has been theoretically studied in Refs. [180, 181, 182, 183, 184, 185, 31] and also recently in GSM [186, 187].

The spectroscopic factor  $[{}^5\text{He}(\text{g.s.}) \otimes p_{3/2}]^{0+}$  in  ${}^6\text{He}(\text{g.s.})$ , calculated in the GSM, is shown in Fig. 12 (top) as a function of the real energy  $e_{p_{3/2}}$ . The spectroscopic factor strongly depends on the position of the  $p_{3/2}$  pole, especially around the 1n-emission threshold in  ${}^5\text{He}$  ( $e_{p_{3/2}}=0$ ). As discussed in Refs. [186, 187], this dependence (in particular, a cusp due to a coupling with the  ${}^4\text{He}+n+n$  channel) follows the threshold behavior of the reaction cross section [175]. Specifically, the anomalous component of the spectroscopic factor *below* the 1n threshold in  ${}^5\text{He}$  behaves as  $(-e_{\ell j})^{\ell-1/2}$ . *Above* the threshold, the spectroscopic factor is complex; the real part behaves as  $(e_{\ell j})^{\ell+1/2}$  while the imaginary part, associated with the decaying nature of  ${}^5\text{He}$ , varies as  $(e_{\ell j})^{\ell-1/2}$ .

Fig. 12 (bottom) illustrates the dependence of spectroscopic factors on the orbital angular momentum  $\ell$  of the transferred nucleon. Here, we consider the  $d_{3/2}$  partial wave in  ${}^{18}\text{O}$  and the spectroscopic factor for the excited  $0_3^+$  state of  ${}^{18}\text{O}$  in the channel  $[{}^{17}\text{O}(3/2_1^+) \otimes d_{3/2}]^{0+}$  (see Ref. [187] for details). The behavior of  $S^2$  is similar to that of  $\langle {}^6\text{He}(\text{g.s.}) | [{}^5\text{He}(\text{g.s.}) \otimes p_{3/2}]^{0+} \rangle$ , except the variations are much weaker and the spectroscopic factor is continuous and smooth; it is its derivative that exhibits a cusp around the  $0d_{3/2}$  threshold. This is again consistent with the general expectation that, for  $\ell=2$ ,  $Re(S^2)$  *below* the 1n threshold of  ${}^{17}\text{O}$  behaves as  $(-e_{\ell j})^{3/2}$  while *above* the threshold  $Re(S^2)$  ( $Im(S^2)$ ) should behave as  $(e_{\ell j})^{3/2}$  ( $(e_{\ell j})^{5/2}$ ).

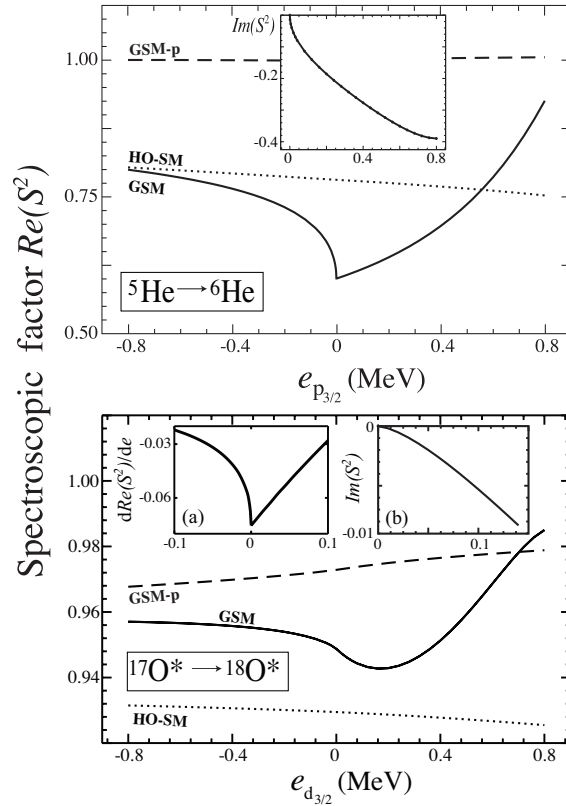


Figure 12: Top: The real part of the overlap integral  $S^2 = \langle {}^6\text{He}(\text{g.s.}) | [{}^5\text{He}(\text{g.s.}) \otimes p_{3/2}]^{0+} \rangle^2$  as a function of the energy of the  $0p_{3/2}$  resonant state.  ${}^6\text{He}(\text{g.s.})$  is bound for all values of  $e_{0p_{3/2}}$ . The solid line (GSM) shows the full GSM result. The dotted line (HO-SM) corresponds to the SM calculation in the oscillator basis of  $0p_{3/2}$  and  $0p_{1/2}$  valence shells, and the dashed line (GSM-p) shows the GSM result in the pole approximation. The imaginary part of  $S^2$  is shown in the inset.  $S^2$  has been normalized so as to be equal to one for vanishing residual interaction. Bottom: Similar to the top portion except for the overlap in the excited  $0_3^+$  state of  ${}^{18}\text{O}$ :  $\langle {}^{18}\text{O}(0_3^+) | [{}^{17}\text{O}(3/2_1^+) \otimes d_{3/2}]^{0+} \rangle^2$ . The first derivative of  $S^2$  in the neighborhood of the  $e_{0d_{3/2}}=0$  threshold is shown in inset (a) while inset (b) displays the imaginary part of  $S^2$ .

To assess the role of the continuum, both resonant and non-resonant, the GSM results are compared in Fig. 12 with the standard SM calculations in a HO basis (HO-SM) and the results of a pole approximation (GSM-p). In contrast to GSM, spectroscopic factors in HO-SM and GSM-p vary little in the energy range considered, and no threshold effect is seen therein. A difference between GSM and GSM-p results illustrates the impact of the non-resonant continuum. Clearly, the continuum coupling should seriously be considered in studies of spectroscopic factors as the associated threshold effects can be as large as those due to, e.g., short-range correlations [188].

In Ref. [187] one-neutron radial overlap integrals were studied in GSM for various energy conditions of parent and daughter nuclei. It was concluded that  $u_{\ell j}(r)$  can be very well approximated by a resonant state of a one-body potential which reproduces the complex generalized one-nucleon separation energy

$$\tilde{S}_{1n}(N) \equiv E(N-1) - E(N) = S_{1n}(N) - \frac{i}{2} [\Gamma(N-1) - \Gamma(N)]. \quad (65)$$

Indeed, the asymptotic behavior of  $u_{\ell j}(r)$  directly depends on  $\tilde{S}_{1n}$  [189, 190]:

$$u_{\ell j}(r) \sim e^{-\kappa r}, \quad r \rightarrow +\infty, \quad \kappa = \sqrt{2m\tilde{S}_{1n}/\hbar}. \quad (66)$$

This is a straightforward generalization of a treatment of one-nucleon overlaps often used in SM studies where a real optical potential is employed with a depth adjusted to reproduce the experimental value of  $S_{1n}$ .

## 6.5 Comparison between GSM and COSM for light nuclei

There have been quite a few applications of the Berggren ensemble to few-body systems. In the context of this review, of particular interest are COSM calculations of Refs. [191, 192]. They considered a complex-scaled Hamiltonian to study light drip-line nuclei such as  ${}^6\text{He}$  and  ${}^{11}\text{Li}$ , described in terms of cluster+valence neutrons systems. The  ${}^9\text{Li}$  core of  ${}^{11}\text{Li}$  is a complex nucleus which was described using a multi-configurational wave function [191]. The use of “V” and “T” types of coordinates in the three-body hybrid-TV model [193] (“V” being related to COSM coordinates and “T” to cluster coordinates) makes it possible to take into account a large number of partial waves within a relatively small configuration space.

$(C_k)^2$	COSM	COSM ( $\ell = 1$ )	GSM
$(0p_{3/2})^2$	1.211-i0.666	1.139-i0.742	1.105-i0.832
$(S1)_{p_{3/2}}$	-0.252+i0.692	-0.119+i0.773	-0.060+i0.881
$(S2)_{p_{3/2}}$	-0.042-i0.026	-0.060-0.031	-0.097-i0.050
sum	0.917	0.960	0.948
$(0p_{1/2})^2$	1.447+i0.007	0.353-i0.077	0.226-i0.161
$(S1)_{p_{1/2}}$	-2.658-i0.042	-0.534+i0.065	-0.198+i0.224
$(S2)_{p_{1/2}}$	1.249+i0.034	0.221+i0.012	0.025-i0.063
sum	0.038	0.040	0.053

Table 3: Components of the ground-state wave function of  ${}^6\text{He}$  in GSM [139] and COSM [194].  $S1$  and  $S2$  indicate configurations with one and two particles in the non-resonant continuum, respectively. The COSM results obtained with partial waves up to  $\ell_{\text{max}}=5$  are displayed in the second column, while the COSM results in a truncated space of  $p_{3/2}$  and  $p_{1/2}$  partial waves are shown in the third column. (From Ref. [194].)

The COSM predictions for the He and O chains [194] have been compared to those of GSM [119, 139]. Table 6.5 shows the ground-state wave function decomposition for  ${}^6\text{He}$  obtained in both approaches. While configurations involving the  $0p_{3/2}$  resonant state are similar, those associated with the  $0p_{1/2}$  broad resonant state are very different. This is due to the large coupling to the non-resonant continuum present in the  $p_{1/2}$  partial wave with a weak contribution of the  $0p_{1/2}$  pole. While GSM is limited to  $p_{3/2}$  and  $p_{1/2}$  partial waves, COSM includes all partial waves up to  $\ell=5$ , so that additional couplings change the relative occupancy of resonant and non-resonant  $p_{1/2}$  shells. This is nicely illustrated in a variant of COSM calculations in which a renormalized interaction was employed in a truncated space of partial waves with  $\ell=1$ . As seen in Table 6.5, GSM and COSM occupations are fairly close in this case [194].

One should stress, however, that the sum of components of the ground-state wave function of  ${}^6\text{He}$  over resonant state and non-resonant continuum states for  $p_{3/2}$  and  $p_{1/2}$  partial waves is practically the same in both GSM and COSM. These quantities give the basis independent estimate of configuration mixing in the ground-state of  ${}^6\text{He}$  as given by GSM and COSM Hamiltonians, respectively. Hence, one can conclude that taking more partial waves does not change quantitatively the prediction about a structure of the ground-state wave function of  ${}^6\text{He}$  [119].

In many aspects, GSM and COSM are complementary. The use of complex-scaled Hamiltonian allows to calculate resonant states in COSM in a basis of discrete bound states. Exact asymptotic behavior, which is efficiently treated by means of hyperspherical coordinates, has to be ensured. In practice, however, this requirement is impossible to fulfill with more than three clusters. This seems to be a major limitation of COSM. The use of overlap method in GSM circumvents this problem, but the price to pay is blurring different emission channels, so that one cannot easily identify different partial widths. This problem is currently under investigation.

## 7 Perspectives

Shell structure is a fundamental property of finite Fermi systems. In nuclear physics, the nucleonic shell structure is characterized by the appearance of large energy gaps in the s.p. spectrum. In open shell nuclei, SM explains the shell evolution in terms of the configuration mixing due to a residual interaction. Experimental discoveries over the last decade, accompanied by theoretical studies, have demonstrated the fragility of the SM concept, in particular the separation of the Hamiltonian into a s.p. potential (that generates shell structure with immutable magic numbers) and a two-body residual interaction [1]. As a result of configuration mixing, new magic numbers in neutron-rich nuclei appear far from stability, while some traditional ones disappear. Another systematic effect of large neutron excess, illustrated in Fig. 1, is a decrease of one-neutron separation energy when moving towards the neutron drip line.

GSM is the OQS formulation of SM for a *self-adjoint* Hamilton operator. This choice offers a number of conceptual advantages. For instance, the transition from a bound to unbound regime, either within a single nucleus or in the long chain of isotopes (isotones), can be viewed as an opening in the configuration space and described without changing the Hamiltonian. The many-body nuclear Hamiltonian in this formulation does not describe just one isolated nucleus ( $N, Z$ ), but all nuclei and all nuclear states that are coupled through various decays and captures. This idealization offers a right physical picture of the many-body system and its interactions.

Already early applications of GSM to the helium chain revealed the essential role of many-body continuum states in the binding mechanism of  ${}^6\text{He}$  (bound),  ${}^7\text{He}$  (unbound), and  ${}^8\text{He}$  (bound). In addition, they demonstrated that the configuration mixing involving continuum space may significantly affect occupancies of different s.p. orbits in many-body states in the vicinity of particle-emission thresholds, thus inducing specific variations of gaps in the spectrum of effective s.p. energies. The resulting picture differs even further from that of the standard SM: the s.p. shell structure probed by GSM becomes a fragile concept in weakly bound nuclei [1]. Studies of many-body wave functions of GSM inform us how subspaces of discrete and scattering states are intertwined. Having a complete basis which allows to describe bound, weakly-bound and unbound states on the same footing is the only way to guarantee the unitarity. This fundamental requirement is not respected in any CQS formulation of the many-body theory. As shown in several examples, restoration of unitarity can strongly affect both values and behavior of spectroscopic factors. The unitarity lies also at the heart of the Wigner threshold effect in the multichannel case. Further consequences of the unitarity restoration on low-energy reactions, mirror symmetry-breaking, pairing correlations, and multi-nucleon decays, deserve further investigations.

Over the last few years, the Berggren ensemble and GSM became an accepted tool for nuclear structure studies. An efficient algorithm for finding discrete resonance states in the non-resonant continuum has been proposed [119] and a new method, based on the application of the DMRG technique, was developed to tame the explosive growth of the Fock space [148]. Recently, the Berggren ensemble has been applied in an *ab initio* description of open quantum systems in a complex-energy coupled-cluster approach [164]. The GSM serves also as a benchmark model to test other approaches to weakly bound states, such as the COSM [194]. Progress has been made in applying Berggren ensembles to the mean-field description of nuclei through Gamow-HFB.

Many challenging problems remain that could be illuminated with GSM — thanks to its ability to follow a quantum transition from a bound-state to unbound regime. For instance, GSM is an excellent tool to explain an ‘alignment’ of a many-body wave function with a channel wave function in the vicinity of a channel threshold [195]. This mechanism, which is a likely source of clustering effects seen near different threshold openings, can be studied in GSM. A near-threshold behavior of pairing correlations is an example from another domain where systematic GSM studies could be most helpful. That is probably a most transparent illustration of a near-threshold clustering.

To improve the detailed description of bound and resonance states spectra in GSM, a development of effective interactions in RHS is an urgent need. This will open a possibility for investigations of configuration-mixing effects involving continuum states in certain isotope chains, e.g.,  ${}^9\text{Li}$  (bound),  ${}^{10}\text{Li}$  (unbound),  ${}^{11}\text{Li}$  (bound), and  ${}^{12}\text{Li}$  (unbound). In this example, GSM could provide a quantitative estimate of admixtures involving coupling of two neutrons (one neutron) with different states of  ${}^9\text{Li}$  ( ${}^{10}\text{Li}$ ) in the ground state of  ${}^{11}\text{Li}$ . Recent experimental studies of the neutron transfer reaction  $p({}^{11}\text{Li}, {}^9\text{Li})t$  [196] provide a strong motivation.



Much effort has been devoted to studies of spectral degeneracies associated with the avoided level crossings, focusing mainly on the topological structure of the Hilbert space and the geometric phases [197, 198]. Among these degeneracies, one finds exceptional points [199, 200, 201] where two eigenfunctions and associated eigenvalues become equal. Up to now, exceptional points have not been studied within RHS. In this respect, GSM could provide a first realistic and consistent many-body framework in which properties of wave functions close to a RHS singularity could be described.

In summary, a complex-energy shell model opens a new window for unification of structure and reaction aspects of weakly bound or unbound nuclear states, based on the open quantum system framework. The developments reviewed here are not solely limited to nuclei; they can be of interest in the context of other open quantum systems in which the coupling to the scattering continuum is present. To describe such systems, one has to give up either the concept of the Hilbert space or the self-adjoint nature of the Hamiltonian if one wants to keep the simplicity and conceptual and practical advantages of the standard SM framework.

## 8 Acknowledgments

Valuable discussions with G. Hagen, A.T. Kruppa, and J. Rotureau are gratefully acknowledged. This work was supported in part by the U.S. Department of Energy under Contract Nos. DE-FG02-96ER40963 (University of Tennessee), DE-AC05-00OR22725 with UT-Battelle, LLC (Oak Ridge National Laboratory, and by the Hungarian OTKA fund No. T46791.

## References

- [1] J. Dobaczewski, N. Michel, W. Nazarewicz, M. Płoszajczak, and J. Rotureau, *Prog. Part. Nucl. Phys.* 59 (2007) 432
- [2] J. Okołowicz, M. Płoszajczak, and I. Rotter, *Phys. Rep.* 374 (2003) 271
- [3] A.M. Lane, and R.G. Thomas, *Rev. Mod. Phys.* 30 (1958) 257
- [4] A.M. Lane, *Nucl. Phys. A* **35**, 676 (1962).
- [5] I.M. Gel'fand and N.Ya. Vilenkin, *Generalized Functions*, Vol. 4, Academic Press, New York (1961)
- [6] K. Maurin, *Generalized Eigenfunction Expansions and Unitary Representations of Topological Groups*, Polish Scientific Publishers, Warsaw (1968)
- [7] A. Bohm, *The Rigged Hilbert Space and Quantum Mechanics*, Lecture Notes in Physics 78, Springer, New York (1978)
- [8] R. de la Madrid, *Eur. J. Phys.* 26 (2005) 287
- [9] G. Ludwig, *Foundations of Quantum Mechanics*, Vol. I and II, Springer-Verlag, New York (1983)
- [10] G. Ludwig, *An Axiomatic Basis of Quantum Mechanics*, Vol. I and II, Springer-Verlag, New York (1983)
- [11] A.F.J. Siegert, *Phys. Rev.* 56 (1939) 750
- [12] R.E. Peierls, *Proc. R. Soc. (London)* A 253 (1959) 16
- [13] J. Humblet and L. Rosenfeld, *Nucl. Phys.* 26 (1961) 529
- [14] P. Lind, *Phys. Rev. C* 47 (1993) 1903
- [15] C.G. Bollini, O. Civitarese, A.L. De Paoli, and M.C. Rocca, *Phys. Lett. B* 382 (1996) 205
- [16] L.S. Ferreira, E. Manglione, and R.J. Liotta, *Phys. Rev. Lett.* 78 (1997) 1640

- [17] R. de la Madrid and M. Gadella, *Am. J. Phys.* 70 (2002) 626
- [18] E. Kapuścik and P. Szczeszek, *Czech. J. Phys.* 53 (2003) 1053
- [19] E. Hernandez, A. Járegui, and A. Mondragon, *Phys. Rev. A* 67 (2003) 022721
- [20] E. Kapuścik and P. Szczeszek, *Found. Phys. Lett.* 18 (2005) 573
- [21] J. Julve, and F.J. de Urries, quant-ph/0701213.
- [22] R. de la Madrid, *AIP Conf. Proc.* 885 (2007) 3
- [23] H.W. Barz, I. Rotter and J. Höhn, *Nucl. Phys. A* 275 (1977) 111;  
I. Rotter, H.W. Barz, and J. Höhn, *Nucl. Phys. A* 297 (1978) 237;  
I. Rotter, *Rep. Prog. Phys.* 54 (1991) 635.
- [24] R.J. Philpott, *Nucl. Phys. A* 289 (1977) 109;  
D. Halderson and R.J. Philpott, *Nucl. Phys. A* 321 (1979) 295; *ibid.* A 359 (1981) 365.
- [25] K. Bennaceur, F. Nowacki, J. Okołowicz and M. Płoszajczak, *J. Phys. G* 24 (1998) 1631 ; *Nucl. Phys. A* 651 (1999) 289 ; *Nucl. Phys. A* 671 (2000) 203 ;  
R. Shyam, K. Bennaceur, J. Okołowicz and M. Płoszajczak, *Nucl. Phys. A* 669 (2000) 65 ;  
K. Bennaceur, N. Michel, F. Nowacki, J. Okołowicz and M. Płoszajczak, *Phys. Lett. B* 488 (2000) 75;  
N. Michel, J. Okołowicz, F. Nowacki and M. Płoszajczak, *Nucl. Phys. A* 703 (2002) 202.
- [26] J. Rotureau, J. Okołowicz, and M. Płoszajczak, *Phys. Rev. Lett.* 95 (2005) 042503 ; *Nucl. Phys. A* 767 (2006) 13
- [27] A. Volya and V. Zelevinsky, *Phys. Rev. Lett.* 94, (2005) 052501 ; *Phys. Rev. C* 74, (2006) 064314
- [28] B. Blank and M. Płoszajczak, *Rep. Prog. Phys.* 71 (2008) 046301.
- [29] G. Gamow, *Z. Phys.* 51 (1928) 204
- [30] R.W. Gurney and E.U. Condon, *Phys. Rev.* 33 (1929) 127
- [31] A.I. Baz, Ya.B. Zel'dovich, and A.M. Perelomov, *Scattering Reactions and Decay in Nonrelativistic Quantum Mechanics*, Israel Program for Scientific Translations, Jerusalem (1969)
- [32] T. Berggren, *Nucl. Phys. A* 109 (1968) 265
- [33] Ya.B. Zel'dovich, *Zh. Eksp. i Theor. Fiz.* 39 (1960) 776
- [34] N. Hokkyo, *Prog. Theor. Phys.* 33 (1965) 1116
- [35] W.J. Romo, *Nucl. Phys. A* 116 (1968) 617
- [36] J. Zimányi, M. Zimányi, B. Gyarmati, and T. Vertse, *Acta Phys. Hung.* 28 (1970) 251
- [37] B. Gyarmati, T. Vertse, J. Zimányi, and M. Zimányi, *Phys. Rev. C* 1 (1970) 1
- [38] J. Bang and J. Zimányi, *Nucl. Phys. A* 139 (1969) 534
- [39] B. Gyarmati and T. Vertse, *Nucl. Phys. A* 160 (1971) 523
- [40] R. Newton, *Scattering Theory of Waves and Particles*, Springer-Verlag, New York, Heidelberg (1982)
- [41] H.M. Nussenzveig, *Causality and Dispersion Relations*, Academic Press, New York (1972)
- [42] J.R. Taylor, *Scattering Theory*, Wiley, New York (1972)

- [43] W. Domcke, *J. Phys.* B 14 (1981) 4889
- [44] V.I. Kukulin, *Theory of Resonances*, Kluwer Academic Publishers, Dordrecht, Boston, London (1989)
- [45] A.B. Migdal, A.M. Perelomov, and V.S. Popov, *Sov. J. Nucl. Phys.* 14 (1972) 488
- [46] H.M. Nussenzveig, *Nucl. Phys.* 11 (1959) 499
- [47] R. Zavin and N. Moiseyev, *J. Phys.* A 37 (2004) 4619
- [48] T. Vertse, P. Curutchet, R.J. Liotta, and J. Bang, *Acta Phys. Hung.* 65 (1989) 305
- [49] R. Id Betan, R.J. Liotta, N. Sandulescu, and T. Vertse, *Phys. Lett.* B 584 (2004) 48
- [50] R. Id Betan, R.J. Liotta, N. Sandulescu, and T. Vertse, *Phys. Rev.* C 72 (2005) 054322
- [51] N. Michel, W. Nazarewicz, M. Płoszajczak, and J. Rotureau, *Phys. Rev.* C 74 (2006) 054305
- [52] N. Dunford and J.T. Schwartz, *Linear Operators*, Wiley Classics Library (1988)
- [53] N. Michel, W. Nazarewicz, and M. Płoszajczak, *Phys. Rev.* C 70 (2004) 064313
- [54] N. Michel, *J. Math. Phys.* 49 (2008) 022109
- [55] A. Mukhamedzhanov and M. Akin, arXiv:nucl-th/0602006
- [56] N. Mukunda, *Am. J. Phys.* 49 (1978) 910
- [57] W.D. Heiss, *J. Phys.* A 37 (2004) 2455
- [58] P.A.M. Dirac, *The Principles of Quantum Mechanics*, Clarendon, Oxford (1958)
- [59] A. Bohm, M. Gadella, and S. Maxon, *Computers Math. Applic.* 34 (1997) 427
- [60] O. Civitarese and M. Gadella, *Phys. Reports* 396 (2004) 41
- [61] G. Garcia-Calderon and R. Peierls, *Nucl. Phys.* A 265 (1976) 443
- [62] Y.B. Zel'dowich, *JETP (Sov. Phys.)* 22 (1961) 542
- [63] E. Hernandez, and A. Mondragon, *Phys. Rev.* C 29 (1984) 722
- [64] E. Hernández, A. Mondragón, and J. M. Velásquez-Arcos, *Ann. der Physik (Leipzig)* 48 (1991) 503
- [65] M.J. Corinthios, *IEE Proc.-Vis. Image Signal Process.*, 150 (2003) 69 ; 152 (2005) 97
- [66] K. Sasada, *Spectral Analysis of the Conductance of Open Quantum Dots*, PhD-thesis, University of Tokyo (2007).
- [67] W.J. Romo, *Nucl. Phys.* A 419 (1984) 333
- [68] T. Berggren, *Phys. Lett.* B 73 (1978) 389
- [69] T. Berggren, *Phys. Lett.* B 373 (1996) 1
- [70] A. Bohm, and M. Gadella, *Lecture Notes in Physics*, Vol. 348, Springer-Verlag, Berlin; A. Bohm, *Int. J. Theor. Phys.* 42 (2003) 2317
- [71] O. Civitarese, M. Gadella, and R. Id Betan, *Nucl. Phys.* A 660 (1999) 255
- [72] A. Bürgers and J-M. Rost, *J. Phys.* B 29 (1996) 3825
- [73] H. Friedrich, *Theoretical Atomic Physics*, Chapter 1, Springer-Verlag, New York (1991)

- [74] J. Bang, F.A. Gareev, M.H. Gizzatkulov, and S.A. Goncharov, *Nucl. Phys. A* 309 (1978) 381
- [75] G. Garcia-Calderon, *Nucl. Phys. A* 448 (1986) 560
- [76] T. Vertse, P. Curutchet, R.J. Liotta, J. Bang, and N. Van Giai, *Phys. Lett. B* 264 (1991) 1
- [77] T. Berggren and P. Lind, *Phys. Rev. C* 47 (1993) 768
- [78] T. Alferova and N. Elander, *Int. J. Quantum Chem.* 97 (2004) 922
- [79] M. Rittby, N. Elander, and E. Brändas, *Lecture Notes in Physics* 325 (1989) 129
- [80] P. Krylstedt, C. Carlsund, and N. Elander, *J Phys.* B 22 (1989) 1051
- [81] B. Milek and R. Reif, *Nucl. Phys. A* 458 (1986) 354
- [82] B. Gyarmati, A.T. Kruppa, and J. Révai, *Nucl. Phys. A* 326 (1979) 119
- [83] F.A. Gareev, M.Ch. Gizzatkulov, and J. Révai, *Nucl. Phys. A* 286 (1978) 512
- [84] T. Vertse, P. Curutchet, O. Civitarese, L.S. Ferreira, and R.J. Liotta, *Phys. Rev. C* 37 (1988) 876
- [85] P. Curutchet, T. Vertse, and R.J. Liotta, *Phys. Rev. C* 39 (1989) 1020
- [86] T. Vertse, P. Curutchet, and R.J. Liotta, *Lecture Notes in Physics* 325 (1989) 179
- [87] G.G. Dussel, R.J. Liotta, H. Sofia, and T. Vertse, *Phys. Rev. C* 46 (1992) 558
- [88] P. Lind, R.J. Liotta, E. Maglione, and T. Vertse, *Z. Phys. A* 347 (1994) 231
- [89] O.I. Tolstikhin, V.N. Ostrovsky, and H. Nakamura, *Phys. Rev. A* 58 (1998) 2077
- [90] K. Toyota, T. Morishita, and S. Watanabe, *Phys. Rev. C* 72 (2005) 062718
- [91] K. Toyota, T. Morishita, and S. Watanabe, *Phys. Rev. C* 63 (2001) 052721
- [92] T. Myo, A. Ohnishi, and K. Katō, *Prog. Theor. Phys.* 99 (1998) 801
- [93] G. Hagen and J.S. Vaagen, *Phys. Rev. C* 73 (2006) 034321
- [94] T. Vertse, K.F. Pál, and Z. Balogh, *Comput. Phys. Comm.* 27 (1982) 309
- [95] L.Gr. Ixaru, *Numerical Methods for Differential Equations*, Reidel, Dordrecht (1984)
- [96] L.Gr. Ixaru, M. Rizea, and T. Vertse, *Comput. Phys. Comm.* 85 (1995) 217
- [97] T. Zhanlav and I.V. Puzynin, *Sov. J. Nucl. Phys.* 55 (1992) 349
- [98] A.T. Kruppa and Z. Papp, *Comput. Phys. Comm.* 36 (1985) 59
- [99] T. Vertse, R.J. Liotta, and E. Maglione, *Nucl. Phys. A* 584 (1995) 13
- [100] J. Blomqvist, O. Civitarese, E.D. Kirchuk, R. J. Liotta, and T. Vertse, *Phys. Rev. C* 53 (1996) 2001
- [101] R.J. Liotta, E. Maglione, N. Sandulescu, and T. Vertse, *Phys. Lett. B* 367 (1996) 1
- [102] N. Sandulescu, O. Civitarese, R.J. Liotta, and T. Vertse, *Phys. Rev. C* 55 (1997) 1250
- [103] T. Vertse, A. T. Kruppa, R. J. Liotta, W. Nazarewicz, N. Sandulescu, and T. R. Werner, *Phys. Rev. C* 57 (1998) 3089
- [104] T. Vertse, A.T. Kruppa, and W. Nazarewicz, *Phys. Rev. C* 61 (2000) 064317

- [105] G.G. Dussel, R. Id Betan, R.J. Liotta, and T. Vertse, *Nucl. Phys. A* 789 (2007) 182
- [106] J. Dobaczewski, W. Nazarewicz, T.R. Werner, J.-F. Berger, C.R. Chinn, and J. Dechargé, *Phys. Rev. C* 53 (1996) 2809
- [107] D.S. Delion and J. Suhonen, *Phys. Rev. C* 61 (2000) 024304
- [108] A. Bianchini, R.J. Liotta, and N. Sandulescu, *Phys. Rev. C* 63 (2001) 024610
- [109] E. Maglione, L.S. Ferreira, and R.J. Liotta, *Phys. Rev. Lett.* 81 (1998) 538
- [110] E. Maglione, L.S. Ferreira, and R.J. Liotta, *Phys. Rev. C* 59 (1999) R589
- [111] K. Rykaczewski, et al., *Phys. Rev. C* 60 (1999) 011301
- [112] A.T. Kruppa, B. Barmore, W. Nazarewicz, and T. Vertse, *Phys. Rev. Lett.* 84 (2000) 4549
- [113] B. Barmore, A.T. Kruppa, W. Nazarewicz, and T. Vertse, *Phys. Rev. C* 62 (2000) 054315
- [114] A.T. Kruppa and W. Nazarewicz, *Phys. Rev. C* 69 (2004) 054311
- [115] I. Martel, M.J.G. Borge, J. Gomez-Camacho, A. Poves, J. Sanchez, and O. Tengblad, *Nucl. Phys. A* 694 (2001) 424
- [116] S. A. Gurvitz, P.B. Semmes, W. Nazarewicz, and T. Vertse, *Phys. Rev. A* 69 (2004) 042705
- [117] R. Id Betan, R.J. Liotta, N. Sandulescu, and T. Vertse, *Phys. Rev. Lett.* 89 (2002) 042501
- [118] N. Michel, W. Nazarewicz, M. Płoszajczak, and K. Bennaceur, *Phys. Rev. Lett.* 89 (2002) 042502
- [119] N. Michel, W. Nazarewicz, M. Płoszajczak, and J. Okołowicz, *Phys. Rev. C* 67 (2003) 054311
- [120] R. Id Betan, A.T. Kruppa, and T. Vertse, *Phys. Rev. C*, in press.
- [121] W.P. Reinhardt, *Ann. Rev. Phys. Chem.* 33 (1982) 223
- [122] J. Aguilar and J. M. Combes, *Commun. Math. Phys.* 22 (1971) 269
- [123] E. Balslev and J. M. Combes, *Commun. Math. Phys.* 22 (1971) 280
- [124] B. Simon, *Commun. Math. Phys.* 27 (1972) 1
- [125] B. Simon, *Phys. Lett. A* 71 (1979) 211
- [126] A. Csótó, B. Gyarmati, A.T. Kruppa, K.F. Pál, and N. Moiseyev, *Phys. Rev. A* 41 (1990) 3469
- [127] R. Lefebvre, *Phys. Rev. A* 46 (1992) 6071
- [128] A.T. Kruppa, R.G. Lovas, and B. Gyarmati, *Phys. Rev. C* 37 (1988) 383
- [129] A.T. Kruppa, P-H Heenen, H. Flocard, and R. J. Liotta, *Phys. Rev. Lett.* 79 (1997) 2217
- [130] A. T. Kruppa, P-H Heenen, and R. J. Liotta, *Phys. Rev. C* 63 (2001) 044324
- [131] C. A. Nicolaides, H. J. Gotsis, M. Chrysos, and Y. Komninos, *Chem. Phys. Letters* 168 (1990) 570
- [132] T.N. Rescigno, M. Baertschy, W.A. Isaacs, and C.W. McCurdy, *Science* 286 (1999) 2474
- [133] J.Zs. Mezei, A.T. Kruppa, and K. Varga, *Few-Body Systems* 41 (2007) 233
- [134] T. Li and R. Shakeshaft, *Phys. Rev. A* 71 (2005) 052505
- [135] Y.K. Ho, *Phys. Rev. A* 19 (1979) 2347

- [136] A.T. Kruppa, R. Suzuki, and K. Katō, *Phys. Rev. C* 75 (2007) 044602
- [137] D. Vautherin and M. Vénéroni, *Phys. Lett. B* 25 (1957) 175
- [138] G. Hagen, M. Hjorth-Jensen, and N. Michel, *Phys. Rev. C* 73 (2006) 064307
- [139] G. Hagen, M. Hjorth-Jensen, and J.S. Vaagen, *Phys. Rev. C* 71 (2005) 044314
- [140] N. Michel, M. Stoitsov, and K. Matsuyanagi, in preparation
- [141] S.T. Belyaev, A.V. Smirnov, S.V. Tolokonnikov, and S.A. Fayans, *Sov. J. Nucl. Phys.* 45 (1987) 783
- [142] N. Michel, W. Nazarewicz, and M. Płoszajczak, *Proc. New Developments in Nuclear Self-Consistent Mean-Field Theories*, YITP, Kyoto, Japan, YITP-W-05-01, B32 (2005)
- [143] R. Id Betan, R.J. Liotta, N. Sandulescu, and T. Vertse, *Phys. Rev. C* 67 (2003) 014322
- [144] S.R. White, *Phys. Rev. Lett.* 69 (1992) 2363; *Phys. Rev. B* 48 (1993) 10345
- [145] J. Dukelsky and S. Pittel, *Rep. Prog. Phys.* 67 (2004) 513
- [146] U. Schollwöck, *Rev. Mod. Phys.* 77 (2005) 259
- [147] E. Carlon, M. Henkel, and U. Schollwöck, *Eur. J. Phys. B* 12 (1999) 99
- [148] J. Rotureau, N. Michel, W. Nazarewicz, M. Płoszajczak, and J. Dukelsky, *Phys. Rev. Lett.* 97 (2006) 110603
- [149] J. Rotureau, N. Michel, W. Nazarewicz, M. Płoszajczak, and J. Dukelsky, in preparation
- [150] N. Moiseyev, P.R. Certain, and F. Weinhold, *Mol. Phys.* **36**, 1613 (1978).
- [151] N. Moiseyev, *Phys. Rep.* **302**, 212 (1998).
- [152] N. Moiseyev, *Chem. Phys. Lett.* **99**, 364 (1983).
- [153] I. McCulloch and M. Gulacsi, *Europhys. Lett.* 57 (2002) 852
- [154] M. Hjorth-Jensen, T.T.S. Kuo, and E. Osnes, *Phys. Rep.* 261 (1995) 125
- [155] K. Suzuki and S.Y. Lee, *Prog. Theor. Phys.* 64 (1980) 2091; K. Suzuki, *Prog. Theor. Phys.* 68 (1982) 246; K. Suzuki, and R. Okamoto, *Prog. Theor. Phys.* 93 (1995) 905
- [156] S. Bogner, T.T.S. Kuo, and A. Schwenk, *Phys. Rep.* 386 (2003) 1
- [157] R. Wiringa, V.G.J. Stoks, and R. Schiavilla, *Phys. Rev. C* 51 (1995) 38
- [158] R. Machleidt, *Phys. Rev. C* 63 (2001) 024001
- [159] E. Epelbaum, *Prog. Part. Nucl. Phys.* 57 (2006) 654
- [160] R.D. Lawson, *Theory of the Nuclear Shell Model*, Clarendon-Press, Oxford (1980)
- [161] R. Balian and E. Brezin, *Nuovo Cim.* 61 (1969) 403
- [162] C.W. Wong and D.M. Clement, *Nucl. Phys. A* 183 (1972) 210
- [163] C.L. Kung, T.T.S. Kuo, and K.F. Ratcliff, *Phys. Rev. C* 19 (1979) 1063
- [164] G. Hagen, D.J. Dean, M. Hjorth-Jensen, and T. Papenbrock, *Phys. Lett. B* 656 (2007) 169
- [165] H.J. Lipkin, *Phys. Rev.* 110 (1958) 1395

- [166] R.R. Whitehead, A. Watt, B.J. Cole, and I. Morrison, *Adv. Nucl. Phys.* 9 (1977) 123
- [167] Y. Suzuki and K. Ikeda, *Phys. Rev. C* 38 (1988) 410
- [168] K. Katō, private communication
- [169] A. Bohr and B.R. Mottelson, *Nuclear Structure*, Vol. 1, W.A. Benjamin, New York (1969)
- [170] N.K. Glendenning, *Ann. Rev. Nucl. Sci.* 13 (1963) 191; N.K. Glendenning, *Direct Nuclear Reactions*, Academic Press Inc. (1983)
- [171] P. Fröbrich and R. Lipperheide, *Theory of Nuclear Reactions*, Oxford Science Publications, Clarendon Press, Oxford (1996)
- [172] M.B. Tsang, Jenny Lee, and W.G. Lynch, *Phys. Rev. Lett.* 95 (2005) 222501
- [173] P.G. Hansen and J.A. Tostevin, *Ann. Rev. Nucl. Part. Sci.* 53 (2003) 219
- [174] A. Gade *et al.*, *Eur. Phys. J. A* 25 (2005) s01, 251; D. Bazin *et al.*, *Phys. Rev. Lett.* 91 (2003) 012501
- [175] E.P. Wigner, *Phys. Rev.* 73 (1948) 1002
- [176] P.R. Malmberg, *Phys. Rev.* 101 (1956) 114
- [177] J.T. Wells, A.B. Tucker, and W.E. Meyerhof, *Phys. Rev.* 131 (1963) 1644
- [178] C.F. Moore *et al.*, *Phys. Rev. Lett.* 17 (1966) 926
- [179] S. Abramovich, B. Guzhovskij, and L. Lasarev, *Sov. J. Part. Nucl.* 23 (1992) 129
- [180] G. Breit *Phys. Rev.* 107 (1957) 1612
- [181] A.M. Lane, *Phys. Lett. B* 33 (1970) 274
- [182] C. Hategan, *Ann. Phys.* 116 (1978) 77
- [183] A.I. Baz, *JETP (Sov. Phys.)* 6 (1957) 709
- [184] R.G. Newton, *Phys. Rev.* 114 (1959) 1611
- [185] W.E. Meyerhof, *Phys. Rev.* 129 (1963) 692
- [186] N. Michel, W. Nazarewicz, and M. Płoszajczak, *Phys. Rev. C* 75 (2007) 031301(R)
- [187] N. Michel, W. Nazarewicz, and M. Płoszajczak, *Nucl. Phys. A* 794 (2007) 29
- [188] W.H. Dickhoff, and C. Barbieri, *Prog. Part. Nucl. Phys.* 52 (2004) 377
- [189] L.D. Blokhintsev, I. Borbely, and E.I. Dolinskii, *Sov. J. Part. Nucl.* 8 (1977) c485
- [190] N.K. Timofeyuk, L.D. Blokhintsev, and J.A. Tostevin, *Phys. Rev. C* 68 (2003) 021601(R)
- [191] T. Myo, K. Katō, S. Aoyama, and K. Ikeda, *Phys. Rev. C* 63 (2001) 054313; T. Myo, K. Katō, S. Aoyama, and K. Ikeda, *Phys. Lett. B* 576 (2003) 281
- [192] T. Myo, K. Katō, and K. Ikeda, *Phys. Rev. C* 76 (2007) 054309
- [193] K. Ikeda, *Nucl. Phys. A* 538 (1992) 355c; S. Mukai, S. Aoyama, K. Katō, and K. Ikeda, *Prog. Theor. Phys.* 99 (1998) 381; Y. Tosaka, Y. Suzuki, and K. Ikeda, *Prog. Theor. Phys.* 83 (1990) 1140
- [194] H. Masui, K. Katō, and K. Ikeda, *Phys. Rev. C* 75 (2007) 034316
- [195] K. Ikeda, N. Takigawa, and H. Horiuchi, *Prog. Theor. Phys. Suppl. Extra Number*, 464 (1968)

- [196] I. Tanihata et al., arXiv:0802.1778
- [197] M.V. Berry, *Proc. R. Soc. London, Ser. A* 392 (1984) 45
- [198] H.-M. Lauber, P. Weidenhammer, and D. Dubbers, *Phys. Rev. Lett.* 72 (1994) 1004; D.E. Manolopoulos and M.S. Child, *Phys. Rev. Lett.* 82 (1999) 2223; F. Pistolesi and N. Manini. *Phys. Rev. Lett.* 85 (2000) 1585; C. Dembowski *et al.*, *Phys. Rev. Lett.* 86 (2001) 787
- [199] T. Kato, *Perturbation Theory for Linear Operators*, Springer Verlag, Berlin (1995)
- [200] M.R. Zirnbauer, J.J.M. Verbaarschot, and H.A. Weidenmüller, *Nucl. Phys. A* 411 (1983) 161
- [201] W.D. Heiss and W.-H. Steeb, *J. Math. Phys.* 32 (1991) 3003